國立臺灣大學電機資訊學院電信工程學研究所

碩士論文

Graduate Institute of Communication Engineering
College of Electrical Engineering and Computer Science
National Taiwan University

Master Thesis

X 頻段金屬氧化物半導體主動雙模環形諧振器帶止濾波器

X Band CMOS Active Dual-mode Ring Resonator Bandstop Filters

黃揚智

Yang-Chih Huang

指導教授：莊晴光 博士

Advisor: Ching-Kuang Tzuang, Ph.D.

中華民國 101 年 6 月

June, 2012

(附件 2)

國立臺灣大學（碩）博士學位論文
口試委員會審定書

X 頻段金屬氧化物半導體主動雙模環形諧振器帶止濾波器
X-Band CMOS Active Dual-Mode Ring Resonator Bandstop Filters

本論文係黃揚智君（R9942026）在國立臺灣大學電信所完成之碩（博）士學位論文，於民國 101 年 6 月 27 日承下列考試委員審查通過及口試及格，特此證明

口試委員：　　（簽名）

（指導教授）

所　　長　　（簽名）

誌謝

不過是兩年半前，碩士班推薦甄試才剛結束，對於未來十分徬徨卻又帶著憧憬的我，決定了未來兩年的實驗室。甫踏進莊晴光老師辦公室的當時，兩旁巍峨的書櫃，以及在辦公室中方桌上討論著對我來說是天書的學長們，讓這一切有如柏拉圖雅典學院般夢幻。當時對於研究的無知與恐懼，讓我覺得開創自己的研究是如此的遙不可及，更遑論碩士論文這般遙遠的里程。

從微波電路、微波積體電路等學科以及 HFSS、ADS 和 Cadence 等入門開始，實驗室的前輩們就彼此互相幫忙，為我在茫然的研究世界中開闢一條前進的道路，並要求我能夠拓展這條道路，讓可能的後繼者能夠更有效率的通過前人的努力，在知識荒原的第一線拓墾。於是在兩年中，第一次的報告、第一次的下線、第一次的量測，逐漸變成了第二次、第三次，然而數字的增大卻是困難減輕，終至最後畢業研究的完成。

能完成這篇論文，首先我要特別感謝我的指導教授莊晴光老師。雖然在一開始，老師給的方向似乎模糊，這一切甚至只是在老師課堂上的一周作業!但是隨著研究的深入，越是發掘此題目背後的課題以及挑戰，不得不佩服老師的遠見。隨著老師在 meeting 上的提問以及評論，這份研究從嘗試變成了清晰的藍圖，然後在慢慢浮現一些結果。同時，老師在各項方面也給予相當多的資源，讓瑣事不會成為研究上的主要難題。同時，順子學長挑起實驗室的運作重責大任，讓我們在研究上有強大的支持，也是功不可沒。

另外，也要感謝口委們在碩士口試上對於這項研究各方面的批評與指教，不同於兩年來熟悉的面孔，這是第一次直接的面對外人的挑戰。口委們對於論文的嚴謹、表達的清晰度甚至於研究的心態與出發點都給予我很多啟發。特別感謝許博文教授對於論文格式的要求與指導，讓我能夠以更精細與嚴謹的角度看待這份工作。感謝吳瑞北教授在很多基礎理論上面的評論以及研究方針上的建議，還有陳毓喬學長對於一些模擬與量測疑點的釐清。因為這些挑戰，讓這份論文能更上一層樓。

當然，實驗室的每一位成員絕對值得我一一感謝。感謝孟霖學長，在我思緒如毛線球時幫我找出了線頭，拉出了這整個研究的主線，學長教導許多系統性的研究方法，並和我討論許多設計上的考量以及濾波器的問題。感謝蘇黎學長，在雙模濾波器方面的研究幫助了我最多，同時給予我許多相當直接的意見，讓我能夠審視自己的研究與

態度。同時學長在研究上的拚勁與學識的淵博，都成為我追逐的重要標竿。星瀚學長幫助我解決許多模擬上遇到的困難以及軟體的問題，並且提供很多有用的建議，同時也要感謝學長多次幫助我量測晶片，使得我得以完成這份論文。感謝昆宏學長以及昭偉學長分別在傳輸線以及主動電路上給我許多指導。感謝俊慶、凱安、凱翔和瑜芝，傳承了許多研究經驗，也帶領我進入碩士生的世界。感謝龍雨、很稱職的一位戰友，陪我一起度過日升日落，一起湊麥當勞外送、分享成果，彼此鼓勵及提醒重要的事。使碩班生涯有著美好的回憶。感謝衍嘉(Johnny)，擴展了我對不同文化的認識，和我一起發掘研究問題，和我一起怨天尤人，在 meeting 過後和我一起在克普魯星區廝殺，甚至到最後發現原來我們的緣分不僅止於此。感謝 551 的同伴們，包括育聰、炫儒、振宇、柏瑋、超塵、書鳴，伴我一起在微波領域披荊斬棘，一起在蘭嶼海洋中悠游浮潛、也一起在召喚峽谷中斬妖除魔。還有吳宗霖實驗室的同學們，包括齊軒、余任、睿智，我們大學緣分不深，卻在研究所有所交集。還有感謝我的室友們，包括小八、致翰、古折、泰禹、祐群，讓我在離開研究室以後有家的感覺，是大學以來最無可取代的夥伴，也很高興我們緣分遠不僅於此。最後感謝家人，給我充足的支持，使我可以心無旁騖，研究可以順利進行。

中文摘要

這篇論文的主題是分析及設計以環型諧振器為主要諧振器的雙模濾波器。本篇論文中的濾波器皆設計在 X 頻段內，並且使用 0.13 微米製程的金屬氧化物半導體技術進行設計。本論文提出的架構，是以一種合成準橫向電磁波模互補式金屬微帶線作為傳輸線結構構成一環型諧振器，並使用指叉式電容對諧振器進行微擾。同時為補償傳輸線阻抗，兩組交錯耦合對被互相垂直地放置於諧振器中以分別補償在雙模諧振器中的兩個模態。本設計使用高度彎曲的傳輸線並以主動電路補償其傳輸能量的損失，所以本文中的濾波器面積非常的小，只有 750 微米見方。此外，由於主動電路補償了傳輸線的損耗，使得諧振器的 Q 值非常的高，因此本設計在阻止帶中擁有很小的反射損失，且有不錯的帶阻效果，加上阻止帶的邊緣非常的陡峭，因此濾波器擁有很高的訊號選擇性。在本論文中，提出三個帶阻濾波器的設計，且三個濾波器的面積均相同。第一個設計擁有非常窄的阻止帶(比例頻寬約為 1%)，且有非常陡峭的頻帶響應。第二個設計為寬頻的雙模帶阻濾波器，頻寬比較寬(比例頻寬約 5%)，阻止帶內也有很小的反射損失及不錯的帶阻效果。第三個設計為雙頻帶的雙模帶阻濾波器。兩個頻帶分別設計在 7GHz 到 7.5GHz 以及 10GHz 到 10.5GHz，在 910 微米見方的面積中，實現兩個具有主動補償的雙模諧振器，達到擁有陡峭邊緣的通帶以及具有小的阻止帶反射損失。在這邊論文中，分別討論有關於不同微擾對於雙模分離的影響及耦合線對於雙模的影響。此外，論文中也討論了雙頻濾波器可能會遇到的問題，並嘗試使用垂直的堆疊結構，以及非對稱或者多條的耦合線。最後，本論文提出模擬和實際實驗的結果，作為驗證。

關鍵字：雙模環型諧振器、交錯耦合對、帶阻濾波器

ABSTRACT

The topic of this thesis is to design and analyze dual-mode ring-resonator-based bandstop filters which are designed to filter out unwanted signals in X band. These filters are fabricated on standard $0.13\mu m$ complementary metal oxide semiconductor (CMOS) process. To implement the dual-mode resonator, a type of artificial synthetic quasi-TEM transmission line called complementary conducting strip (CCS) is used to construct a ring resonator with an inter-digital capacitor load on the resonator as a perturbation. In these designs, transmission lines are highly meandered, and the total area of these filters are equal or less than $750\mu m \times 750\mu m$ or $0.03\lambda_0 \times 0.03\lambda_0$, which is a very small area. Besides, two cross-coupled pairs are put orthogonally to compensate the losses of two modes in the resonator, respectively. The Q factor of the resonator is very high and therefore these filters can achieve low return loss and good rejection level with a very sharp bandstop response. There are three designs proposed in this thesis. The first one is designed to achieve very narrow bandwidth (1% of fractional bandwidth) and a very steep bandstop response. The second design offers wider stopband bandwidth (4% of fractional bandwidth). The third is a dual-band dual-mode bandstop filter which implemented two resonators in the area of $910\mu m \times 910\mu m$, also with narrow bandwidth and sharp response. In this thesis, some issues to design the dual-mode filter are discussed, like the relation between perturbation and mode splitting and the effect of the coupled line. On the other hand, some special strucutures of dual-band dual-mode filter are also discussed, such as the vertical stacked transmission line, multi-metal coupled line and asymmetric coupled line. At last, the simulation and measurement results are shown as well.

Key Words: dual-mode ring resonator, cross-coupled pair, bandstop filter.

CONTENTS

LIST OF FIGURES

LIST OF TABLES

Chapter 1 Introduction

1.1 Motivation

Nowadays, communication devices are more and more common and popular around the world. Besides, mobile instruments are more and more functional and complicated. While the space of the instrument is not changed, the desire of a more compact communication system has increased. The dual-mode filter usually forming a narrowband response by exhibiting two resonances with closed frequencies simultaneously in a single physical structure, has the advantages of compact sizes and high selectivity, has been widely used as the component of communication system. Though the dual mode phenomenon has first been studied on the waveguide for a long time ago, the first planar dual mode resonator was not proposed until 1972 by Wolff[1]. In the paper, Wolff proposed a dual mode ring resonator in which a perturbation, or discontinuity, was put on the ring resonator to split the two degenerate modes. However, planar dual mode resonator has not been widely studied until 1990 by Guglielmi and Gatti[2], who claimed that the response of a planar ring resonator dual-mode BPF with symmetric configuration is quasi-elliptic response. The various type of dual mode filter then has been studied on bandpass filter, including annular slotline[3], open-loop[4] , patch[5, 6] or E-shaped resonator[7-11].

The traditional active filters are implemented by operation amplifiers[12]. The first dual mode amplifier was first proposed in [13], which implementing two single-ended GaAs FETs to compensate the loss of microstrip lines by the negative resistance of the FETs. In that paper, a 2.16% fractional bandwidth and 0-dB insertion loss while preserving excellent shape of the response. During now, the active bandpass has been implemented on CMOS, achieving 0-dB insertion loss and very small area at

24 GHz[14].

Comparing to the bandpass filters, which are commonly used in microwave system to suppress unwanted signals, bandstop filters are has less attention. However, bandstop filters still have some potential to play a role in the communication system.

For example, bandstop filters can be applied in designing wide-band bandpass filters and also multi-band filters. Also, in some cases a bandstop filter is suitable in rejecting undesired signal in order to enhance robustness in communication systems with some costs in loss or phase delay due to the finite out-band return loss of the bandstop filter.

More, from the research results of microwave active filters up to date, an active bandstop filter also shows more practicality than a bandpass one in some aspects. For an active bandpass filter, power is an important issue, the output power of the filter may suffer from the limitation of the active circuit. For an active bandstop filter, the desired signals passing through the signal line are less attenuated due to the high linearity of the active bandstop filter. Therefore, multiband and wide-bandwidth bandstop filter may have great application. Up to today, microstrip dual-mode bandstop filters using microstrip triangular patch resonators with a rectangular slit as a perturbation[15-18], E-shaped resonator [7-11] and ring resonator [13, 19-21]have been proposed. The bandstop filters now can achieve dual-band-dual-mode response and are of great potentialities.

To filter out the unwanted signals, a very wide-band filter or multiband filter are needed in communication system. The bandstop filters can be cascaded to achieve this goal with the coast of increasing the circuit size.

Complementary -oxide-semiconductor (CMOS) process is now a very important technology in electronic devices. CMOS can offer very accurate and low cost circuit

designs with active component available easily. In 0.13 μm CMOS process, the metal wire of the top metal can be of width only 0.21 μm and have the distance between two lines at the same order. Besides, CMOS can provide more than 7 metal layers process in 0.13 μm technology and with via connecting each layer, which make the design more flexible. On the other hand, the full-EM simulation tool is developed for a long time and is now accurate and convenient enough for general engineer. With the CAD software and general used computers, to design the circuit on CMOS chip is more and more popular since its accuracy and cheap for massive production.

Despite of the advantages of CMOS fabrication, there are also some issues to be conquered. Since the thickness of the metal layer is so thin and the semiconductor substrate is usually doped, the conductor loss and dielectric loss are high compared to PCB. The quality factor of a normal passive transmission line in CMOS is usually less than 10 in 10 GHz. To design a passive bandstop filter in 10 GHz, the in-band rejection is about only 3dB or less due to the high losses and thus low Q factor of the resonator. One main purpose of investigating active filter design is to compensate ohmic loss of passive filters, especially when the loss is very high. For example, a cross-coupled pair providing differential negative resistance can be integrated to a resonator, promoting the Q factor of the resonator and thus forming a active filter topology[14]. Thanks to the maturity of CMOS technology, the active components can be put under the passive structure and will not change the total area of the filter. The loss issue can be solved and the active bandstop filter on IC chip is possible.

To reduce the total area of the filter, the resonator must be highly meandered. There is a kind of synthetic quasi-TEM transmission lines called complementary-conducting-strips transmission lines(CCS TLs)[22-24]. The CCS TL provides good isolation between meandered lines and higher slow wave factor than

microstrip line. It has been applied on active bandpass filters[14, 24-26]. Also in those designs, near 0-dB insertion loss has been implemented on CMOS fabrication.

The theory and technique will be developed in this thesis for designing a dual-mode bandstop filter with 0-dB in-band return loss and high selectivity on CMOS. Also it is interesting to find some design issues and phenomenon of the dual-mode resonator in bandstop filters. Those considerations give rise the research of active dual-mode bandstop filters.

1.2 Focus of This Thesis

In this thesis, the main object is to implement the bandstop filters with loss compensation. Some features are listed below:

1. To design a miniaturized bandstop filter with $0.0300\lambda_0$ periphery length in highly meandered transmission lines and coupled lines, and also with capacitive loads to reduced the transmission line length.
2. To achieve low in-band loss of resonator. The return loss in band can be compensated to less than -3.00 dB dB by implementing a very high Q resonator. The Q of the filter is exceeding 85 in the first design.

In the thesis, a bandstop filter with very small area (about $0.030 \times 0.030\ \lambda_0^2$) is implemented. Also by vertically stacking the resonators, a dual-mode dual-band bandstop filter implementing in the same area is also shown as well

1.3 List of Contributions

The contributions arising from this thesis are as follows:

1. A small area dual-mode bandstop filter is implemented on CMOS facrication.
2. A vertically stacked dual-band dual-mode filter is demonstrated with a small area identical to the single band one.
3. Demonstrate an application of the CCS TLs and shows the flexibility and good isolation characteristic.
4. Use the cross-coupled pair to compensate the loss of the transmission line and as perturbation as well. Also discuss the effect and trade-off relation of the transistor size, linearity and perturbation effect.

1.4 Outline of the Thesis

There are five chapters in this thesis. The content of every chapter is described below:

In chapter 2, some background knowledge is described. First some definition and response of filters are mentioned. The dual-mode resonator history is well introduced. Some research is discussed in more detail. There is also a section which takes a look at the evolution of active filters with compensation. Still some basic properties and discussion about active filters are introduced in the last of this chapter.

Chapter 3 introduces the detail and design flow of designing a dual-mode bandstop filter. First the conventional complementary-conducting-strip transmission line (CCS TL) is shown in detail. Also in this section the parameters of the transmission line used

in the designs of this thesis is shown. Then, the loss compensation circuit is explained and the effect of the circuit to the resonator is discussed. On the other hand, the dual mode behavior of the ring resonator with the transmission line characteristic and capacitor position is found out. The discussion of the position of transmission and reflection zeros is in this section too. Then the implementation and measurement result of the edge-coupled and broadside coupled dual-mode bandstop filter is shown in detail.

Chapter 4 discusses some issues and design flow of the dual-band dual-mode bandstop filter. The mesh ground of the CCS TLs and signal line is discussed. The coupled line is also introduced. The effect of the two resonators to each other is also mentioned. The simulation and measurement result is at the last.

Chapter 5 is the conclusion of this thesis, and the reference is put at the last of this thesis.

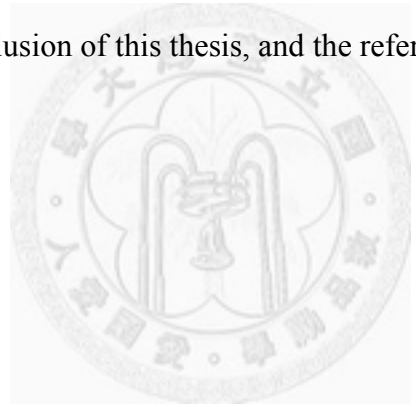

Chapter 2 Microwave Filter and Dual-mode Resonator

2.1 Microwave Filters

In classical microwave filter designs, transfer function of the filter is considered. The transfer function of a two-port filter describes network response characteristics. It is also a mathematical expression of S_{21}. In many cases, a transfer function for a lossless passive filter network is defined as (2.1)

$$\left|S_{21}(j)\right|^2 = \frac{1}{1+\varepsilon^2 F_n^2(\Omega)} \tag{2.1}$$

Where ε is a ripple constant, $F_n(\Omega)$ is a filtering or characteristic function, and Ω is a frequency variable.

For a given transfer function, the insertion loss can be expressed as

$$IL(\Omega) = -20\log\frac{1}{\left|S_{21}(j\Omega)\right|^2} dB \tag{2.2}$$

On the other way, we have $|S_{11}|^2 + |S_{21}|^2 = 1$ for a lossless and passive two-port network, the return loss is computed as

$$RL(\Omega) = -20\log\left[1-\left|S_{21}(j\Omega)\right|^2\right] dB \tag{2.3}$$

There are some common types of filter function introduced below. Those filters are with transmission zeros, ripples and rejections. Although in some cases the responses of the filters are not always match the pure mathematical forms, they are still important to describe and compare the performance of filters.

2.1.1 Chebyshev Function Filters

If the insertion loss of a filter can be expressed as

$$IL(\Omega) = 10\log\left(1+\left|K(s)\right|^2\right) \tag{2.4}$$

where the characteristic function $1+\left|K(s)\right|^2$ is called power loss ratio. For a non-zero $K(s)$, the insertion loss is always larger than 0dB. In Chebyshev filters, this function is called the Chebyshev function.

The Chebyshev function has all transmission zeros in infinity and equal-ripple in-band response. The characteristic function is defined by

$$\left|K(j\omega)\right|^2 = \varepsilon^2 T_n^2\left(\frac{\omega}{\omega_c}\right) \tag{2.5}$$

The polynomial $T_n(x)$ is the Chebyshev polynomial of nth-degree. Here are some properties of $T_n(x)$

1. T_n is even of n is even, and is odd if n is odd.
2. All zeros of T_n are in the interval $-1 < x < 1$.
3. The ripple of $\mathrm{T_n}$ is always between ± 1 in the interval $-1 < x < 1$.
4. T_n always go through $(1,1)$.

While $|x| \le 1$, T_n can be expressed as

$$T_n(x) = \cos\left(n\cos^{-1}x\right) \tag{2.6}$$

If $|x| > 1$,

$$T_n(x) = \cosh\left(n\cosh^{-1}x\right) \tag{2.7}$$

2.1.2 Elliptic Function Filters

While the Chebyshev response has equalripple in the passband, the elliptic

function has equalripple in both the passband and stop band. This response has the steepest side response of the passband. The characteristic function of a elliptic filter is

$$\left|K\left(j\omega\right)\right|^2 = \varepsilon^2 R_n^2\left(\frac{\omega}{\omega_p}, L\right) \tag{2.8}$$

Where $R_n\left(\frac{\omega}{\omega_p}, L\right)$ is a rational function, and has characteristics below,

1. R_n is even (odd) if n is even (odd).
2. R_n has all its n zeros in the interval $-1 < \omega/\omega_p < 1$ and all its n poles are outside that interval.
3. R_n oscillates between values of ± 1 in the interval $-1 < \omega/\omega_p < 1$.
4. R_n must go through $(1,1)$.
5. $1/R_n$ oscillates between values of $\pm 1/\mathrm{L}$ in the interval $|\omega| > \omega_s$.

$R_n(x, L)$ is defined through the differential equation:

$$\left(\frac{dR_n\left(x,L\right)}{dx}\right)^2 = M^2\frac{\left(R_n^2-1\right)\left(R_n^2-L^2\right)}{\left(1-x^2\right)\left(x^2-x_L^2\right)} \tag{2.9}$$

or

$$\frac{CdR_n}{\sqrt{\left(R_n^2-1\right)\left(R_n^2-L^2\right)}} = \frac{Mdx}{\sqrt{\left(1-x^2\right)\left(x^2-x_L^2\right)}} \tag{2.10}$$

Where C and M are constants. This is the differential equation for the Chebyshev function, and its solution involves elliptic integrals. This rational function is derived and expressed as

$$R_n\left(x,L\right) = C_1 x\prod_{\nu=1}^{(n-1)/2}\frac{x^2-sn^2\left(2\nu N/n\right)}{x^2-\left[x_L/sn\left(2\nu N/n\right)\right]^2} \quad for\ n\ being\ odd \tag{2.11}$$

$$R_n(x,L) = C_2 x \prod_{\nu=1}^{n/2} \frac{x^2 - sn^2\left((2\nu-1)N/n\right)}{x^2 - \left[x_L / sn(2\nu N/n)(N/n)\right]^2} \quad for\ n\ being\ even \tag{2.12}$$

Here $sn(2\nu N/n)$ is the Jacobian elliptic function and N is the complete elliptic integral of the first kind defined by

$$N = \int_0^{\pi/2} \frac{d\xi}{\sqrt{1-k^2\sin^2\xi}} \tag{2.13}$$

Where k is the modulus of the elliptic integral. The modulus is less than unity for k to be real, permitting an alternative definition of k where

$$k = \sin\theta = \frac{\omega_p}{\omega_s} \tag{2.14}$$

where θ is the modular angle. By substituting for x, x_L and k shown before, the characteristic function for n odd is expressed as

$$\left|K(j\omega)\right| = \varepsilon C_1 \frac{\omega}{\omega_p} \prod_{\nu=1}^{(n-1)/2} sn^2\left(\frac{2\nu K}{n}\right) \frac{\omega^2 - sn^2\left(\frac{2\nu K}{n}\right)\omega_s^2 \sin^2\theta}{\omega^2 sn^2\left(\frac{2\nu K}{n}\right) - \omega_s^2} \tag{2.15}$$

2.1.3 Quasi-Elliptic Function Filters

The elliptic function filter has all transmission zeros at finite frequencies. This kind of filter has a better cutoff rate in the transition region. The characteristic function is now

$$\left|K(j\omega)\right|^2 = \varepsilon^2 F_n^2(\omega_{a,}\omega) \tag{2.16}$$

The generalized Chebyshev function is expressed as

$$F_n(\omega) = \cosh\left[\cosh^{-1}\omega + (n+1)\cosh^{-1}\left(\omega\sqrt{\frac{\omega_a^2-1}{\omega_a^2-\omega^2}}\right)\right] \tag{2.17}$$

The transmission zeros are of order $(N-1)$ at $\omega = \pm\omega_a$ and one at infinity. Another similar form of the transfer function is given by

$$F_n(\omega) = \cosh\left[(n-2)\cosh^{-1}\omega + \cosh^{-1}\left(\frac{\omega\omega_a - 1}{\omega_a - \omega}\right) + \cosh^{-1}\left(\frac{\omega\omega_a + 1}{\omega_a + \omega}\right)\right] \quad (2.18)$$

2.2 Microwave Dual-Mode Filters

As mentioned in chapter 1, the first dual-mode filters are waveguide filter with some discontinuity to disturb the waveguide. The planar dual-mode resonator is first studied by I. Wolff in 1972[1]. In the paper, the ring resonator has a perturbation to split the degenerate modes. As shown as Figure 2.1, Wolff proposed two types of mode-splitting mechanism. In Figure 2.1, the left figure is the first one. The input and output coupling is asymmetric to the resonator. The right figure is the other one, which has symmetric input/output coupling but has a cutting notch on the resonator.

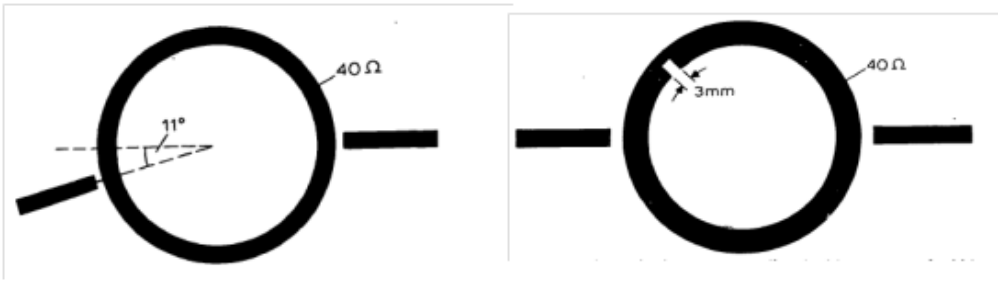

Figure 2.1 Two types of mode splitting mechanism of ring resonator.

The popular used structure of dual-mode bandpass filter is proposed by M.Guglielmi and G. Gatti[2]. The input and output coupling is separated by 90° line of the resonator. The structure is shown in Figure 2.2. The paper shows some experimental results. Besides, in the paper the two transmission zeros are considered and used to realize high out-band rejection. The response of the filter is like the quasi-elliptic

function response.

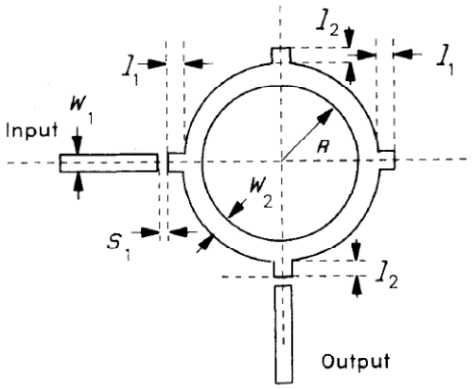

Figure 2.2 The dual-mode bandpass filter by M.Guglielmi and G. Gatti.

There are also other type of dual-mode resonators that has been studied, such as squared patch [6], triangular patch[15-18], and E-shaped resonator[7] [7-11].

It is known that the two fundamental modes in ring resonator without perturbation are degenerate modes. These two modes are also orthogonal and uncoupled. While there are perturbation or discontinuities, the two modes may be coupled. In [17], J.S. Hong discussed about the relationship between perturbation size and resonant frequency splitting.

Most of the studies of dual-mode resonators are first used in bandpass filters. In [27], A. Guror described the coupling types of the degenerate mode of the dual-mode resonator. In [27], different kinds of perturbation are put on the corner of square ring resonators. He stated that in some cases the response is the Chybeshev response with no transmission zeros be observed. In other cases, the response of the bandpass fitler exhibits as elliptic characteristic with a pair of transmission zeros. However, the paper is commented by S. Amari[28]. S. Amari stated that the former response is not a Chebyshev response, but still an elliptic response with two transmission zeros lying not on the imaginary axis of the complex plane.

Though most of the characteristic are first be discussed on bandpass filters, most types are now also used to implement the bandstop filter, such as triangular types[17], E-shaped[7] , ring resonator[19] and squared ring resonator with perturbation[21, 29], as shown in Figure 2.3.

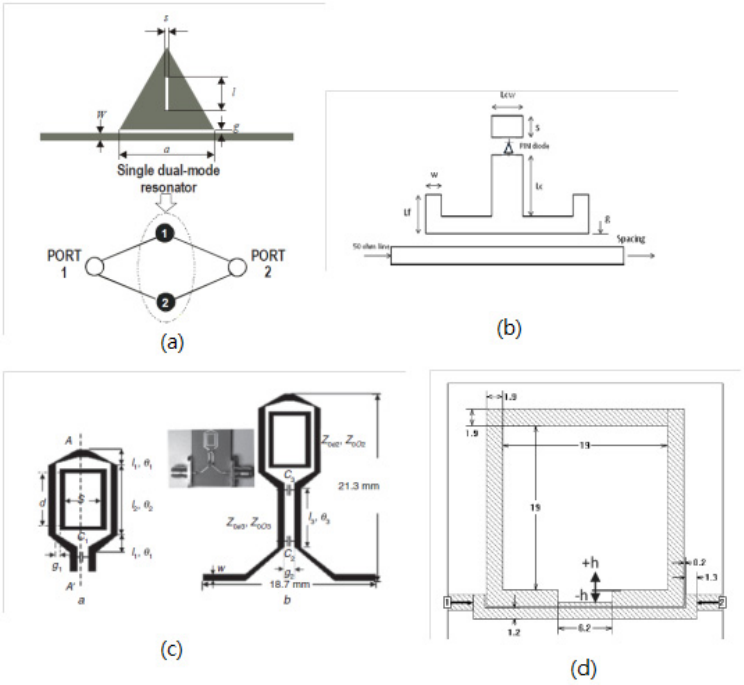

Figure 2.3 Dual-mode bandstop filters. (a) Triangular patch dual mode resonator filter[17]. (b) E-shaped dual mode resonator filter[7]. (c) Ring dual-mode resonator filter[19].(d) Ring dual-mode resonator filter with perturbation stub.[29]

Dual-band dual-mode bandstop filter has also been implemented in 2009[21]. The layout is shown as Figure 2.4. The line is coupled by two dual-mode ring resonator. In this paper, the resonant frequency and the position of reflection zeros are discussed, and most of the characteristic can be tuned by the parameters in the layout of Figure 2.4.

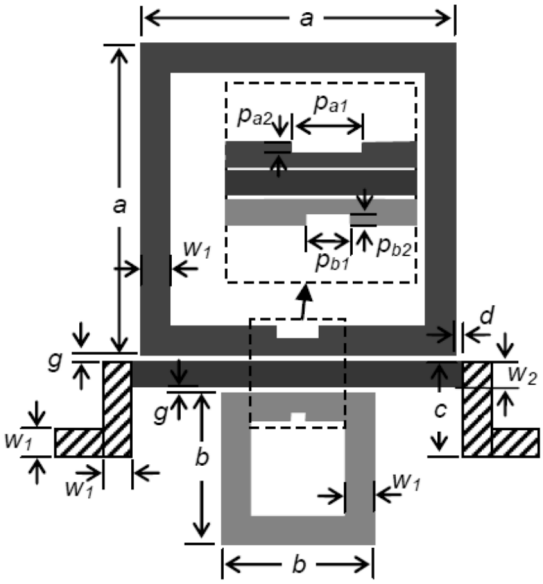

Figure 2.4 Dual-band dual-mode bandstop filter.[21]

2.3 Active Filters

In the past, the active filters can be implemented by operation amplifier [8]. However, the operation amplifier is implemented by active component and the structure is complex; therefore, the operation frequency is too low. The semiconductor technology is not as good as recent years. Thus, this kind of filters is hard to design as microwave filters. On the other hand, the loss in integrated circuit(IC) is too large, the Q factor of the transmission line is too low so that purely passive structure without compensation may suffer from significant insertion losses.

Some methods are proposed to compensate the loss. One of which is the inverted collector transistor configuration. While looking into the transistor from emitter, the transistor can be viewed as an inductor with a negative resistor. In order to get the pure negative resistor, a capacitor can be put parallel to the transistor to cancel the inductor. This LC tank circuit can be used as a single-ended compensation device and used in

filter design. On the other hand, there is another method to cancel the inductor without using lumped capacitor. In this method, a segment of transmission line as a resonator connects to the transistor directly. This method has better tolerance control than the lumped circuit [29].

Instead of single ended compensation circuits, there are also differential compensation circuits being proposed [30]. In the paper, cross-coupled pair is used to compensate the transmission line based resonator. The differential compensation circuit has some advantages, like noise immunity and second harmonic rejection.

The first active compensated dual-mode bandpass filter is proposed by U. Karacaoglu in 1996 [9]. Figure 2.5 shows the schematic of this filter. The single-ended compensation circuit is used to compensate the loss of the ring resonator. This active bandstop filter has 2.16% fractional bandwidth with 0-dB insertion loss in band.

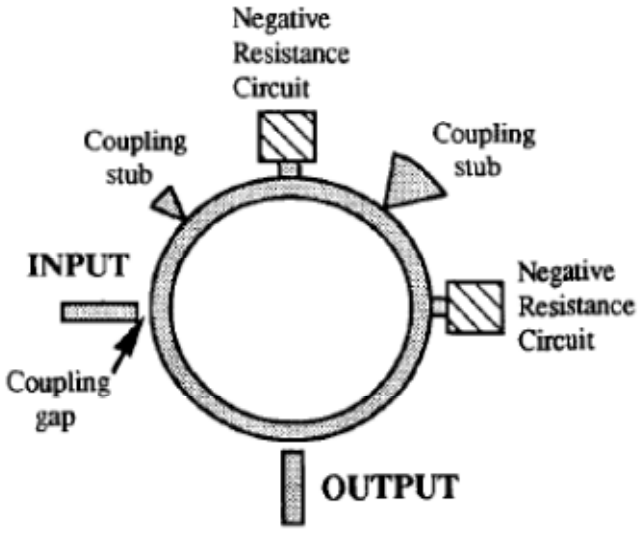

Figure 2.5 Active dual-mode bandpass filter.

The first active dual-mode bandpass filter fabricated on monolithic IC is proposed in 2012[31]. This work uses the cross-coupled pair as a differential compensation circuits. The resonator in this paper is ring type. Figure 2.6 shows the schematic of the

total filter and compensation circuit. The fractional bandwidth is about 3.86%. The insertion loss is 0dB with excellent shape of response being preserved. Until now, no active dual mode bandstop filter is implemented on CMOS IC.

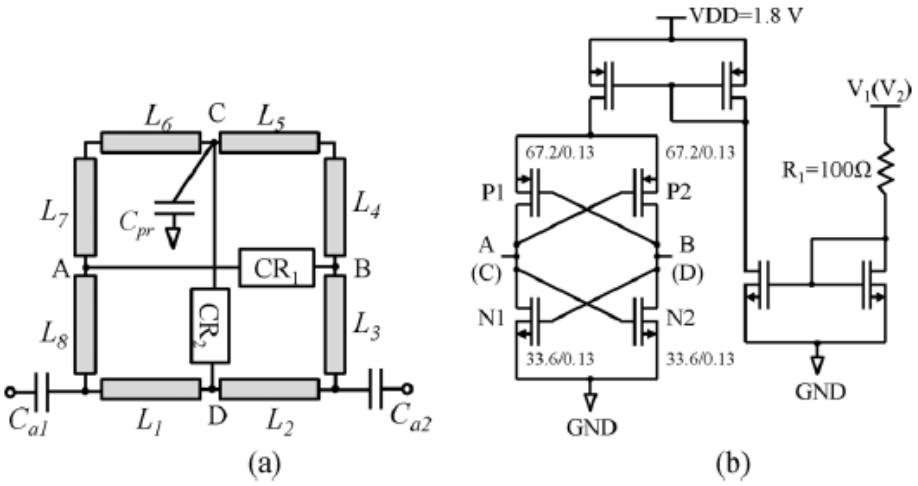

Figure 2.6 Active dual-band bandpass filter on CMOS fabrication. (a) Schematic of the filter. (b) The circuit of compensation circuit.

Until now, no active dual mode bandstop filter is implemented on CMOS IC.

2.4 Some Considerations of the Dual-Mode Active Filters

In this section, some properties is introduced to measure a bandstop filter characteristics. Including the S-parameter shaped, in-band return loss and out-band insertion loss, non linear behavior and power consumption.

As defined in section 2.1, the insertion loss is

$$IL(\Omega) = -20\log\frac{1}{\left|S_{21}(j\Omega)\right|^2} \tag{2.19}$$

And the return loss is

$$RL(\Omega) = -20\log\left[1-\left|S_{21}(j\Omega)\right|^2\right] \tag{2.20}$$

For an ideal bandstop filter, the insertion loss in the stop band is infinite and the return loss is zero. However, out of the stop band, all the signal should pass through the filter without loss. The insertion loss is zero and the reflection loss is infinite. Besides, the harmonic resonance is sometimes undesirable and should be discussed.

For the bandstop filters, the out-band loss (insertion loss) and in-band rejection level are the most important concerns. However, in real cases, the transmission line is not lossless. In-band rejection level should be discussed with the out-band insertion loss to make more sense. In this thesis, the bandwidth is defined as the $|S_{21}|$ is less than -10dB. The skirt factor is a measure for the steep range of two sides of stop band. Since the out-band loss cannot be compensated in the design in this thesis, the skirt factor reference cannot be set to be too high. In this thesis, the skirt factor is viewed as a measured of the steepness of the side of stop band from -5dB to -10dB. Therefore, the skirt factor is defined as

$$\mathrm{SF} = \frac{\mathrm{BW}_{-5\mathrm{dB}}}{\mathrm{BW}_{-10\mathrm{dB}}} \tag{2.21}$$

Noise is an important issue for microwave systems. The noise response should be considered especially in the active devices. The measure for the noise response is the noise figure, defined as

$$\mathrm{NF} = \frac{\mathrm{SNR}_{\mathrm{in}}}{\mathrm{SNR}_{\mathrm{out}}} \tag{2.22}$$

Where SNR is defined as

$$\mathrm{SNR} = \frac{\mathrm{P}_{\mathrm{signal}}}{\mathrm{P}_{\mathrm{noise}}} \tag{2.23}$$

However, in the design of this thesis, the active circuit only contributes to the rejection in the stopband. For the desired signal in the system, the filter act as a pure passive component. The NF is actually the out-band insertion loss. Therefore, the NF will not be discussed in the measurement results analysis.

Since an active circuit is used in the design, the linearity issue can be concerned. When the undesired signal in stopband passes the filter, it will be attenuated by the filter. However, while the input power increases, the rejection level will change due to the nonlinearity of transistors. The measure of this nonlinearity issue is the input P1dB. Input P1dB is the input power level when the rejection level degrades 1dB. In this thesis, the simulation results of P1dB is about -23dBm.

Chapter 3 Active Dual-mode Bandstop Filter

3.1 Overview

To reduce the area, the transmission lines of the resonator must be meandered lines. In the designs in this thesis, a kind of synthetic quasi-TEM transmission line, called complementary-conducting-strip transmission lines (CCS TL) is used. This kind of guiding structure provides high slow wave factor as well as good isolation between meandered signal lines. Some details of CCS TLs will be described in this chapter.

On the other hand, there are many differences in designing passive structures on printed circuit board (PCB) and on CMOS chip. One of the most significant difference is the transmission line loss. In lower microwave frequencies (several giga hertz), the Q factor of the CMOS transmission line is quite low compared to those fabricated on PCB cases. For the cases in this thesis, if the structure is purely passive, the performance is so bad that it is not like filters. However, one of the advantages of CMOS technology is that it is easy and convenient to achieve many transistors in the circuit. Thus, active compensation circuits are applied to the resonator to enhance Q factor. In the stop band of the filters, the Q can be compensated to very high and such that $S_{11} \approx 0\text{dB}$. Besides, the active circuit offers parasitic capacitors which may affect the behavior of the resonators, and can be used to achieve dual mode. The detail issues of designing the active issue will also be introduced in this chapter.

Figure 3.1 is the total schematic of the proposed dual-mode active bandpass filter. Figure 3.1(a) shows a capacitor-perturbed (C_{pr}) and cross-coupled-pair-loaded ring resonator. The energy passes one of the coupled lines and some is coupled into this resonator from the coupled line on the top. The cross-coupled pair 1 is connected to the

resonator on point A and point C. The cross-coupled pair 2 is connected to the resonator on point B and point D. The transmission line length $L_1 = L_2 = L_3 = 1.65$ mm. The coupled line length $L_4 = 1.71$ mm. Figure 3.1(b) is the cross-coupled pair circuit. P1, P2 are PMOS transistors and N1, N2 are NMOS transistors. The gate of one PMOS is connected to another PMOS's drain and vice versa. The NMOS circuit is complementary to the PMOS circuit and forms a complementary cross-coupled pair together. V_{bias} is around 0.9V. Figure 3.1(c) is the layout of the dual-mode active bandstop filter. The size of a CCS TL unit cell is $30\mu m \times 30\mu m$.The total size is $750\mu m \times 750\mu m$.

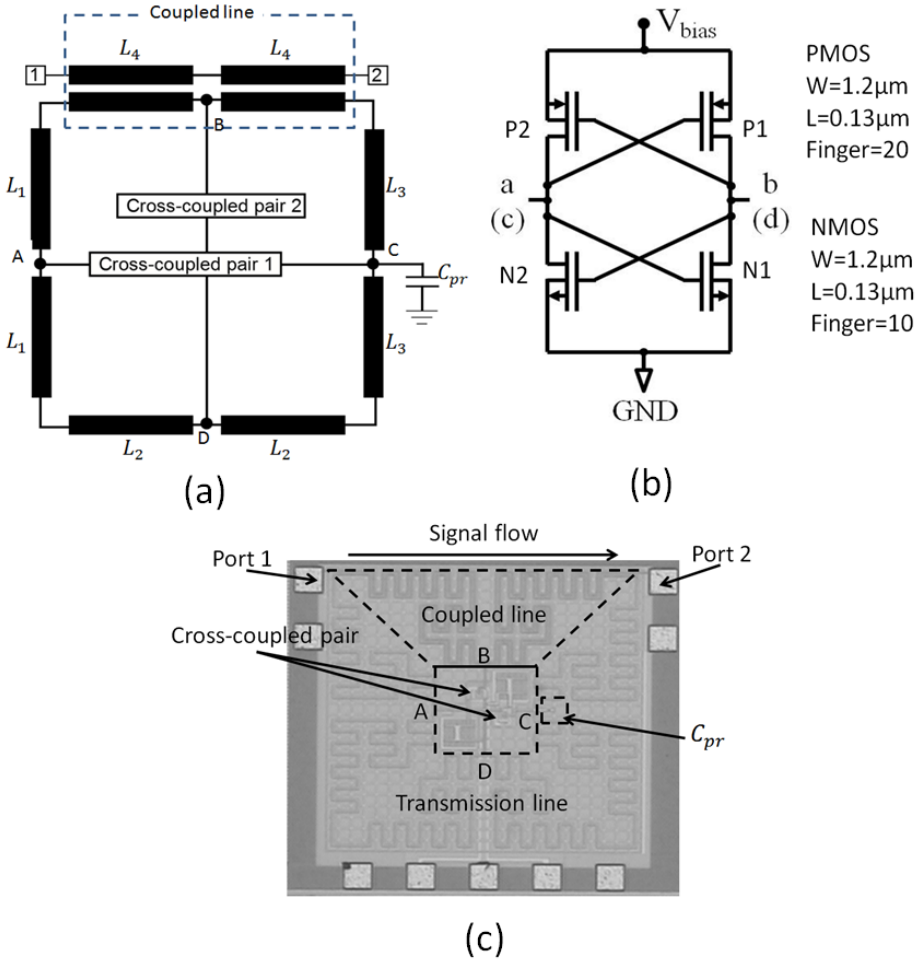

Figure 3.1 Schematic of the proposed dual-mode active bandpass filter. (a) A capacitor-perturbed (C_{pr}) and cross-coupled-pair-loaded ring resonator. The energy passes one of the coupled lines and some is coupled into this resonator from the coupled line on the top. The cross-coupled pair1 is connected to the resonator on point A and point C. The cross-coupled pair2 is connected to the resonator on point B and point D. $L_1 = L_2 = L_3 = 1.65$ mm. $L_4 = 1.71$ mm. (b) The cross-coupled pair circuit. P1, P2 are PMOS transistors and N1, N2 are NMOS transistors. V_{bias} is around 0.900 V. (c) Layout of the dual-mode active bandstop filter. The size of a CCS TL unit cell is 30.0 μm × 30.0 μm.

3.2 Synthetic Transmission Lines

As mentioned above, to reduce the area, the transmission line must be meandered. The conventional complementary-conducting-strip transmission lines (CCS TLs) are one type of synthetic quasi-TEM transmission lines, and is adopted in these designs of bandstop filters as transmission lines. The CCS TLs support the quasi-TEM mode of EM wave propagation.

Figure 3.2 shows the 3D structure and design parameters of a CCS TLs. In the 3D view, one can find that the ground is a periodic structure. The figure on the bottom of figure3.1 is the unit cell view of CCS TLs. ***P*** is the periodicity, which is much smaller than the wavelength of guiding wave. S is the width of the linking line between each cell. B is the patch width in the middle of the unit. This kind of structure can been viewed as a periodically combination of two type guiding structures: elevated co-planer waveguides(CPW) and microstrip lines(MS). The left part of Figure 3.3 is the cross-sectional view of A-A' cut, and is very similar to microstrip line structure. This performs as a locally capacitance region. The right part of Figure 3.3 is the cut view of B-B' line, and it shows an elevated co-planer waveguide structure, performing as a high-impedance inductive region. Noticed that in the sectional drawing of B-B’ line, the middle patch is constructed from the bottom metal layer to the top one. However in the designs of this thesis, the patches contain only the top metal layer.

The whole unit cell is composed of a mesh ground part and signal line part. Each part of CCS unit cell makes difference in some basic coefficients of transmission line, such as electrical length, transmission impedance and loss.

There are some advantages using CCS TLs, especially in IC fabrication. First, CCS ground offers sufficient good isolation between adjacent signal lines. Besides, the

effect of corners is not significant. Once the coefficients of CCS unit cell have been chosen, the CCS can be easily achieved by arranged unit cells with desired length and pass, while corners will not make big difference in length. This leads to a simpler method to design the whole transmission line without doing EM simulations all the time, which may take much time. On the other hand, thanks to the good isolation between adjacent lines, the whole meandered line can be more compact. Moreover, in IC fabrication, DRC rules have to be matched before tape-out. By using CCS TLs, it is much easier to meet the metal density rules, which is an important issue on IC fabrication. Last, CCS TLs have high slow wave factor, which means that on the same frequency, CCS TL can achieved by less length than other guiding structure.

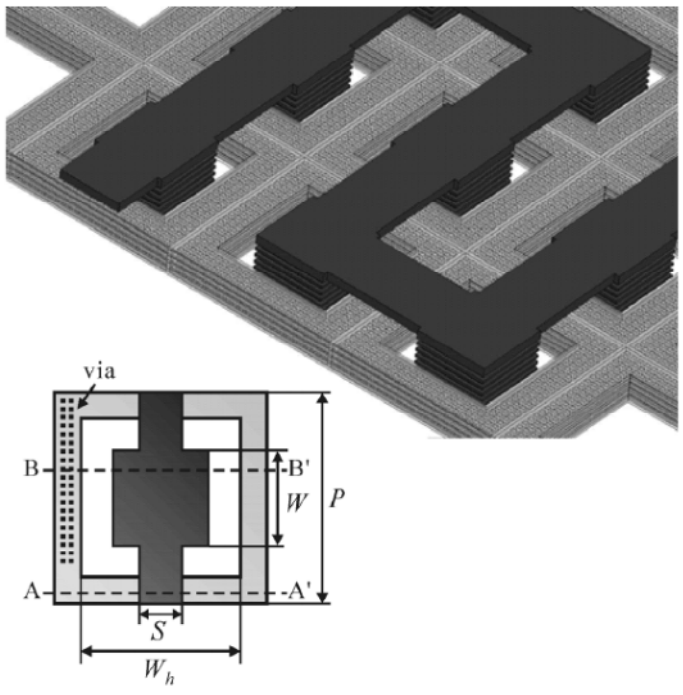

Figure 3.2 The 3D-view of CCS TL and its unit cell

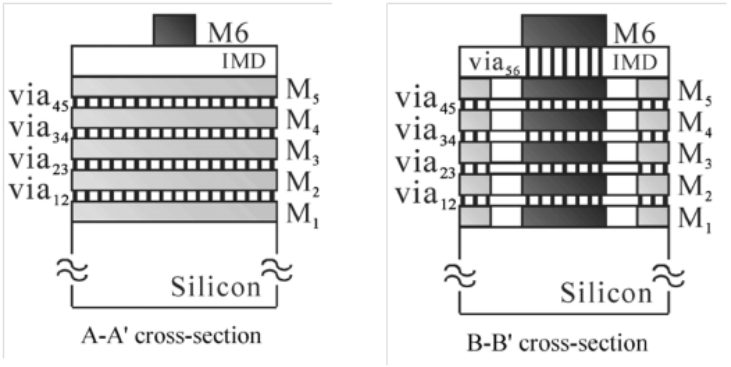

Figure 3.3 Cross-section view of CCS unit cell.

In this thesis, the resonating frequency is around 10 GHz. P is choose as 30 μm; W is chosen the same as S, which is 6 μm; W_h is 26 μm. The whole signal line are on the top metal layer (UTM). The S-parameters of CCS TLs are simulated on Ansys HFSS 12.0. The parameter of the transmission line is found by the equation below:

$$Z_C = Z_0 \sqrt{\frac{(1+S_{11})^2 - S_{21}^2}{(1-S_{11})^2 - S_{21}^2}} \tag{3.1}$$

$$e^{\gamma L} = \frac{1 - S_{11}^2 + S_{21}^2 + \sqrt{(1+S_{11}^2 - S_{21}^2)^2 - S_{21}^2}}{2S_{21}} \tag{3.2}$$

$$Q = \frac{\beta}{2\alpha} \tag{3.3}$$

$$SWF = \frac{\beta}{\beta_0} \tag{3.4}$$

Where Z_C is the characteristic impedance of the transmission line, γ is the propagation constant. Q is the quality factor and SWF is the slow wave factor. The characteristic impedance of CCS transmission line is $53.5 - j2.50\ \Omega$. The slow wave factor is 2.11, which is higher than $\sqrt{\varepsilon_r}$ of the dielectric layer in CMOS. The quality factor Q is 9.53, which is low compared to those transmission lines on PCB, and thus a

compensated circuit is applied to compensate the loss of transmission lines.

3.3 Active Compensation Circuit

The transmission line loss of advanced CMOS fabrication is so significant that purely passive structure will not work well as the same design on PCB board. As mentioned in chapter 2, there are some techniques to compensate the loss. In this thesis, one type of differential compensation circuits, called cross-coupled pair, is used. Figure 3.4 shows a cross-coupled pair and its T-model. In Figure 3.4 (a), a and b connect to two sides of resonator. On resonating frequency, we can calculate the Z_{in} between A and B points by T-model, as shown in Figure 3.4 (b). V_t and I_t are the voltage and current of an virtual source put between A and B, respectively. The two transistors are substituted by T-model. We have

$$V_t = -I_t \times \frac{2}{g_m} \tag{3.5}$$

$$Z_{in} = \frac{V_t}{I_t} = -\frac{2}{g_m} \tag{3.6}$$

From the simple derivation above, we can view the cross-coupled pair offering negative resistance. Therefore, the whole cross- coupled pair can be seen as a parallel negative resistor with two shunt capacitors which is provided by the C_{gs} and C_{gd} of every transistors in the circuit. Also we know that a resonator can be seen as a capacitor parallels an inductor. If the resonator has losses, there should be a parallel resistor too. To combine the resonator and cross-coupled pair, we have the equivalent circuit, as shown in Figure 3.5.

(a) (b)

Figure 3.4 Cross-coupled pair: (a) Schematic. (b) The small signal model of cross-coupled pair.

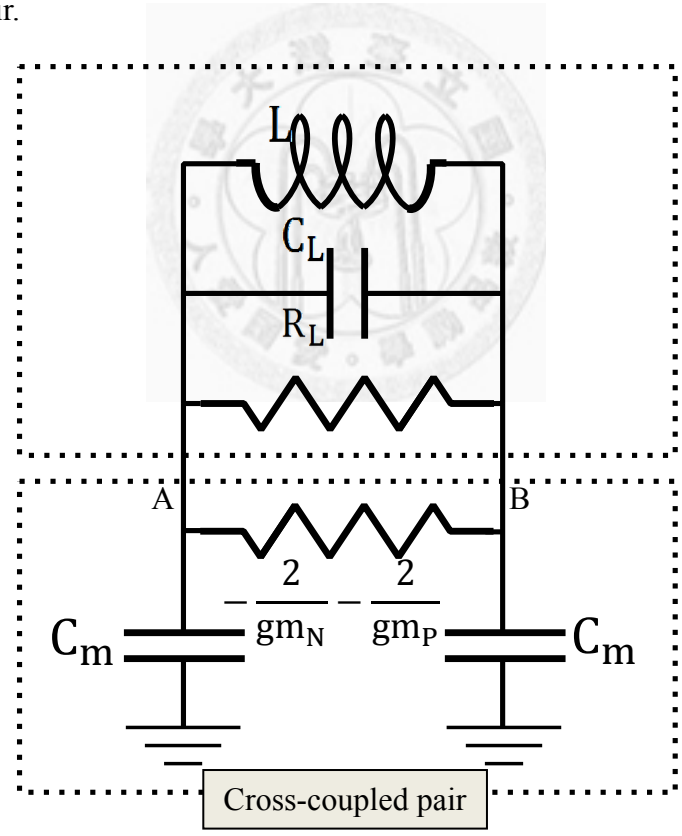

Figure 3.5 The equivalent model of a half-wavelength resonator with cross-coupled pair.

If $\frac{-2}{g_m}$ and R_L are equal and therefore eliminated, the loss of the resonator can be

compensated. Notice that $C_{gs} + C_{gd}$ can be substituted as a shunt capacitor between A and B in Figure1.3, and the value of that capacitor is $(C_{gs} + C_{gd})/2$. Those capacitors can be combined with the capacitors of the resonator C_L, and affect the resonance frequency as well.

3.4 The Q-enhanced Ring Resonator

In discussion of [33], the cross-coupled pair shown as Figure 3.4 (a) can only amplify the differential-mode signal. For common-mode signal, it acts like a load since the positive feedback will not occur. With the case in [33], a cross-coupled pair is to compensate a half-wavelength CCS TL. However, in this cases, the cross-coupled pair is loaded on the ring resonator, as the case in [10]. As discussed in [10], two cross-coupled pair are put on the resonator. In the consideration of simplification, each cross-coupled pair is designed to compensate only one mode on resonating frequency. Besides, the cross-coupled pair only works under odd mode in two ends. The position of the cross-coupled pair must meet the resonance condition of the resonator. It is know that the fields of the two modes are orthogonal. Therefore, it is reasonable to put the two cross-coupled pairs orthogonally. In this dissertation, the cross-coupled pairs are put to the 0°, 90°, 180° and 270°, respectively, of the resonator as differential compensation circuits, which is shown in Figure 3.6.

The parasitic capacitors of the cross-coupled pair, as shown as $C_{gs} + C_{gd}$ in Figure 3.7, can be the perturbations of the resonator. L is the group wavelength at the resonance frequency or λ_g. The capacitor $C_{gs} + C_{gd}$ is determined by the sizes of the transistors in the cross-coupled pairs. However, the transistor sizes also change the g_m

with the same biasing voltage. For a bigger transistor, the parasitic capacitor is bigger, and it needs lower biasing voltage to offer the same g_m. Nevertheless, the big transistor may suffer from the problem of linearity. Therefore, choosing the size of the transistors is a trade-off and concern between resonance frequency, supplied voltage and linearity.

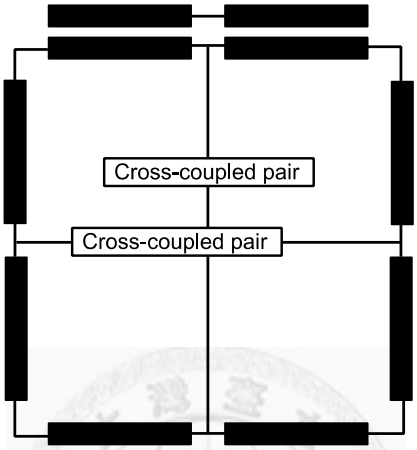

Figure 3.6 A ring resonator with two cross-coupled pairs to compensate the loss.

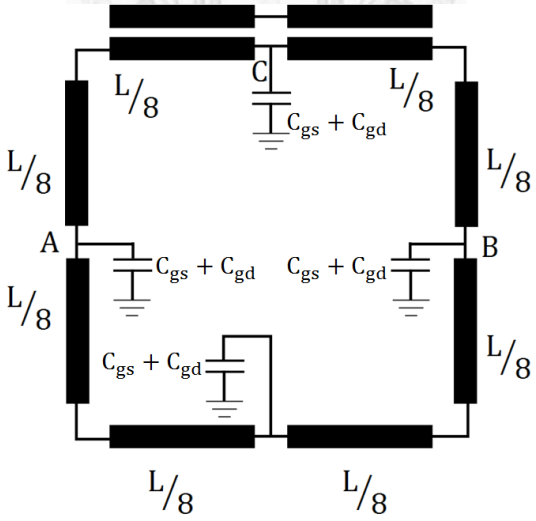

Figure 3.7 Equivalent circuit of the Figure 3.6. Noticed that the transmission line is now lossless since the compensation circuit. L is the group wavelength at the resonance frequency or λ_g.

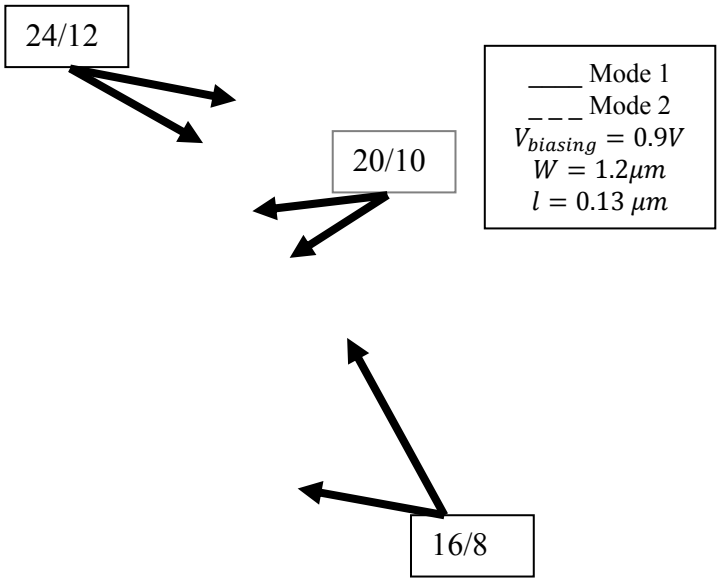

Figure 3.8 The compensation of the cross-coupled pair with different transistor size for each mode. The solid line is mode1. The dotted line is mode2. The channel length of the transistor is 0.13 μm. The width is 1.20 μm. The transistor size is labeled in the figure. The first number is the finger number of PMOS transistor and the second number is the finger number of NMOS transistor.

Figure 3.8 is the full-EM simulation results of compensation by two cross-coupled pairs individually. In the figure, S_{11} is used to measure the central frequency and the compensation of the cross-coupled pairs. The solid line shows the case while each one mode is compensated with different size of transistors in the cross-coupled pair. The dotted line is the other mode being compensated by other cross-coupled pair with different transistors sizes. The supplied voltage to the cross-coupled pair (see Figure 3.8 (a)) is fixed to 0.90 V for all the case. It is clearly to

see that while the transistor become bigger, the resonance frequency gets lower. On the other hand, the g_m increases while the size gets bigger. In the last, it is found that only one mode is compensated while only one cross-coupled pair is on. The schematic in figure3.5 is proved to meet all the requirements above.

The definition of the quality factor (Q factor) is the ratio of total storage energy in the resonator and the dissipation rate of the energy, as below

$$Q = 2\pi \frac{P_{storage\ in\ resonator}}{P_{dissipation\ per\ time}}. \tag{3.7}$$

For an unloaded resonator, which denotes a resonator without any input and output loads, the Q factor is called unloaded Q factor. If the resonator is connected to an external load, the load also contributes to the dissipation. The ratio of the storage and the dissipation rate from the external load is the external Q factor. The total Q factor of the schematic can be written as

$$\frac{1}{Q_{total}} = \frac{1}{Q_{unloaded}} + \frac{1}{Q_{external}} \tag{3.8}$$

From 3.8, one can find that Q_{total} is equal or less than Q_{unload}. One of the advantages of active resonator is the very high Q factor (exceeding 100). Therefore Q_{total} can achieve a very high value. In Figure 3.8, Q_{total} of transistor with finger number 24 for PMOS and 12 for NMOS and $V_{biasing}$=0.90 V is 34. The Q_{total} can be higher while increasing $V_{biasing}$. For smaller transistor, the $V_{biasing}$ can be higher to get the same Q factor.

The bandwidth of the active bandstop filter can be quite narrow. In this thesis, a 1%- fractional-bandwidth dual-mode bandstop filter is proposed.

3.5 Dual-Mode Ring Resonator

3.5.1 Resonate Frequency of the Dual-mode Resonator

It is well known that there are two degenerate modes occurring in a ring resonator. For the fundamental resonating mode, the wavelength is equal to the total length of the ring resonator. As stated by Wolff, when some perturbations are put on the resonator or asymmetrically feed are applied to the resonator, the two modes may not degenerate anymore. The resonator becomes a dual-mode resonator.

As introduced in chapter 2, if we feed the energy into the resonator by two capacitors, the response is a bandpass filter, as shown in Figure 3.9(a). One the other hand, if we feed the resonator by a coupled line, the response is a bandstop filter, as shown in Figure 3.9(b). One of the most important things for the bandstop or bandpass filters is the central frequency of concerning band. The central frequency is also the resonating frequency of the resonator. For a dual mode resonator, it can be treat as two resonator, each have different resonating frequency. In this section, the resonating frequencies of the resonator and the reflection zeros will be discussed.

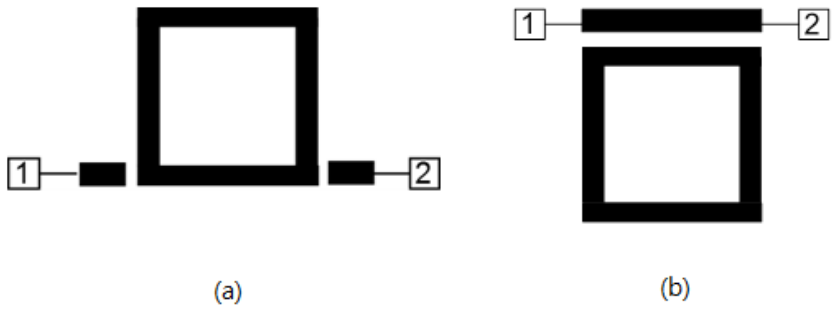

Figure 3.9 (a) Bandpass filter (b) Bandstop filter.

In section 3.3, the equivalent circuit of the resonator with cross-coupled pairs is shown in Figure 3.7. For easily discussed, the figure is redrawn as Figure 3.10. The only

difference between Figure 3.7 and Figure 3.10 is that C_{pa} now replaces $C_{gs} + C_{gd}$. Each of the capacitor, with the value C_{pa}, is separated by $L/4$ transmission line. L is the total length of the ring resonator. The two segments of the top transmission lines are actually coupled lines. However, the length of the couple line is chosen that on the resonating frequency, the electric length is $L/8$ for each segment.

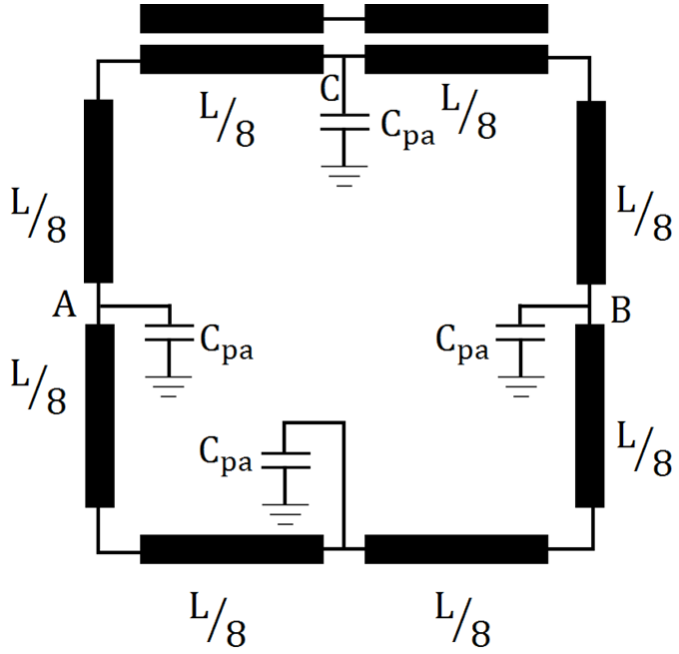

Figure 3.10 The equivalent circuit of the resonator with cross-coupled pairs. L is the group wavelength at the resonance frequency or λ_g.

For this structure, one can get the analytic solution by computing the *ABCD* matrix. For example, if we start from A and go clockwise, the structure can be viewed to be eight part cascaded, as depicted in Figure 3.11.

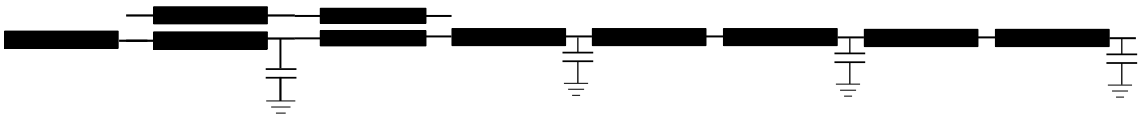

Figure 3.11 The schematic of the resonator splitting form the point A in Figure 3.10.

It is known that for a cascade system, the total *ABCD* matrix can be gotten by multiplying each *ABCD* matrix directly. The boundary condition of the resonance is that both voltage and current are continuous in phase everywhere on the resonator. Therefore if we assume that the whole *ABCD* matrix of figure3.9 is $\boldsymbol{X}$, we have

$$\boldsymbol{X}\begin{bmatrix}\mathbf{v}\\ \mathbf{i}\end{bmatrix} = \begin{bmatrix}\mathbf{v}\\ \mathbf{i}\end{bmatrix}$$

Where

$$\boldsymbol{X} = (\boldsymbol{TLC})(\boldsymbol{LTC})(\boldsymbol{T^2C})^2$$

The $\boldsymbol{T}$ is the *ABCD* matrix of a transmission line segment. $\boldsymbol{L}$ is the *ABCD* matrix of a coupled line segment. $\boldsymbol{C}$ is the *ABCD* matrix of the shunt capacitor. By solving the eigenequation of $\boldsymbol{X}$ corresponding to eigenvalue 1, the resonating frequency van be obtained. However, this is a tedious work and the form is too complicated to find the relationship between each parameter.

Instead of solving the eigenequation discussed above, the structure is simulated by Agilent Advanced Design System 2009. For this structure, both the coupled line and capacitors can be seemed as perturbations.

First, the coupled line effect is discussed. In this design, there are three parameters that affect the response directly: even mode characteristic impedance (denoted by Z_e), odd mode characteristic impedance (denoted by Z_o) and the electrical

length of the coupled line. Assume that there is not any capacitor loaded to the resonator. The characteristic impedance of the transmission line is 50 Ω. If the electrical length is fixed, the effect of the transmission line is determined by the even and odd mode impedance of the coupled line. If the even mode and odd mode impedance is higher, the equivalent impedance of the coupled line is higher, and the coupled line looks like as a perturbation. Like the capacitor case, while the equivalent impedance of the coupled line is very low, there will two transmission zeros before the second harmonic. If the equivalent impedance gets higher and higher, there is indeed no transmission zero and with only a minimum in $|S_{21}|$. The structure acts as a single mode or degenerate mode resonator. While the equivalent impedance is much higher, two transmission zeros will occur and the resonator becomes dual mode resonator again.

Now the effect of the capacitor is considered. It is known that the two solutions of the ring resonator, or two modes, are orthogonal. To simplify the cases, the capacitors are only added at 0°, 90°, 180° and 270°. Since the cross-coupled pairs is used to compensate the losses, there are four capacitors at 0°, 90°, 180° and 270° in our designs. In order to control the dual modes position, a capacitor may be added to change the mode separation. There are three cases in this design, as shown in Figure 3.12.

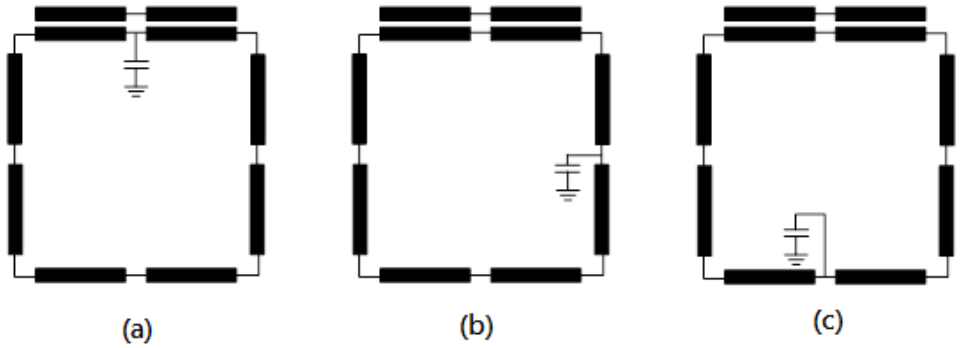

Figure 3.12 Three cases of the capacitor perturbation.

In Figure 3.12(a), the capacitor is added to the middle of the coupled line. This makes the coupled line an asymmetric coupled line. It's harder to analyze this case, but in fact the effect of adding capacitor like Figure 3.12(a) is similar to the case in Figure 3.10(c). The cases in Figure 3.12(a)(c) the capacitor is loaded to one mode of the ring resonator. Therefore, while the capacitor is loaded, the frequency of one of the mode will decrease. However, in Figure 3.12(a), the reflection zeros are changed very differently from the case of figure3.10(c). The reflection zeros are transmission poles, and will make different in the performance of $|S_{21}|$. In the case of Figure 3.12(b), the capacitor is loaded to a different mode. With the increasing of this capacitor, one of the transmission zeros will move to lower frequency.

3.5.2 Reflection Zeros

In the previous discussion, the effect on $|S_{21}|$ of the coupled line and the loaded capacitors is mentioned. Now the $|S_{11}|$ is concerned. The structure in this thesis has transmission zeros and reflection zeros as well. The response is like a quasi-elliptic response with reflection zeros are at finite and infinite as well. The $|S_{11}|$ zeros occur while there exists at least one energy flow loop in the structure.

Like $|S_{21}|$ case, it is possible to get the theoretical solution for the reflection zeros. See Figure 3.13, It is possible to compute the Y matrix of the coupled line (denoted as $\mathbf{Y_b}$) and the other $3/4$ loop of the resonator(denoted as $\mathbf{Y_a}$). For the total Y matrix $\mathbf{Y_{total}}$, $\mathbf{Y_{total}} = \mathbf{Y_a} + \mathbf{Y_b}$. The reflection zeros occur while y_{11} of $\mathbf{Y_{total}}$ equal to zero.

To see the outcome more insight, the position of the reflection zero is also depend on the design of the coupled line and capacitors. First the coupled line is discussed. To

maintain the whole length of the resonator, there will be a reflection zero at the frequency as if the coupled line acts like a half length resonator. This is due to the source load coupling. For example, if the electric length of the coupled line is 90° on 10 GHz, there will be a reflection zero on 20GHz. While the characteristic impedance changes, the reflection zeros might occur near the stop band.

The relation between capacitors and reflection zeros is very complicated. The reflections zeros controlled by capacitors exist beside the stop band. If a reflection zero occurs, it may move with the stop band, or the transmission zero with the value changes of a capacitor. The reflection zeros may merge into one if they are too adjacent and may be cancelled by transmission zeros. The behavior of the $|S_{11}|$ should be confirmed by EM simulation.

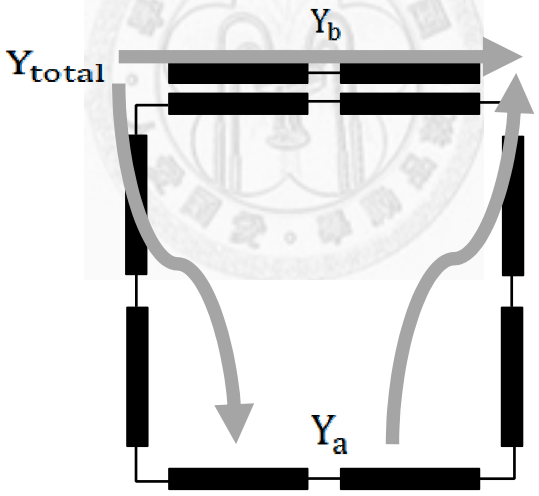

Figure 3.13 Y-matrix calculation for the bandstop filer.

3.6 Harmonic responses of the bandstop filter

In the discussion of the above sections, the position of the resonance frequency and reflection zeros has been clear. Figure 3.14 is the full-EM simulation from 1GHz to 20GHz. The stop band is at 8.5GHz and the second harmonic is suppressed.

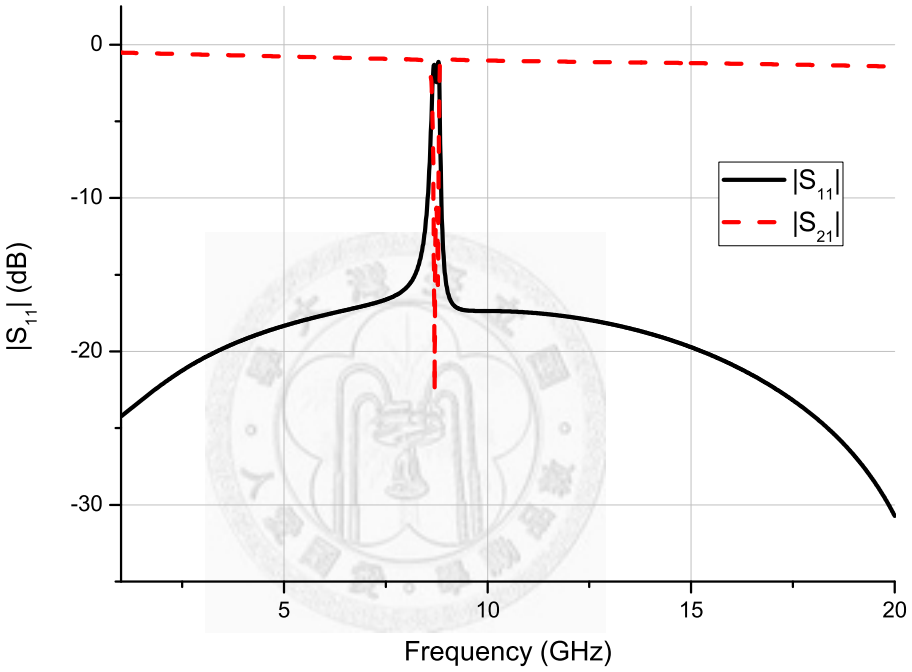

Figure 3.14 The wide band response of the dual-mode bandstop filer.

There are several reasons that the second harmonic does not exist. First, as mentioned before, the loss of the transmission line is so large that it is hard to design a purely passive filter. The loss compensation circuit is the cross-coupled pair, which is a differential compensation. It offers negative resistances only if the two ends are odd mode. In the schematic shown in Figure 3.6, the modes of even order harmonic will be even across a half resonator. The cross-coupled pair will not compensate the even-order

harmonic. To that mode, the crossed coupled pair looks like a load. Therefore it's hard to see the second harmonic.

Another reason is the electrical length of the coupled line. The coupled line is 90° on the resonance frequency. This makes a reflection zeros occur at the second harmonic. The transmission zeros and reflection zeros can cancel each other. However, since there are some capacitors load the on the resonator, the frequencies of the reflection zeros and second harmonic might not be at the same frequency. This method to eliminate second harmonic is not an effective way.

The third harmonic is now be concerned. The third harmonic can be compensated by cross-coupled pair, and there is no reflection zero on third harmonic. However, for every different mode, the needed g_m is different, and thus the biasing voltages have to be adjusted to meet the requirement. The biasing voltage is meet the demand of the fundamental mode, and it cannot compensate the third harmonic well. The third harmonic indeed exists, but is not obvious. The higher order harmonics suffer from the effect of the capacitors which move the harmonic frequencies and reflection zeros in a complicated form, and is hard to be analyze.

3.7 Implementation of Active Bandstop Filter

3.7.1 Active Dual-mode Bandstop Filter with Edge-coupled Line

In the previous discussion, the CCS TLs, cross-coupled pair and some properties have been studied. These contribute to the design of the active dual mode bandstop filter. Figure 3.15(a)shows the schematic of the bandstop filter. Figure 3.15(b) is the circuit of the cross-coupled pairs. All the length of the transistor is chosen as $0.130\ \mu m$. The

width of transistors is 1.20 μm. The figure numbers of the pmos and nmos are 20 and 10 respectively since the mobility of electric holes is approximate twice as the mobility of free electron.

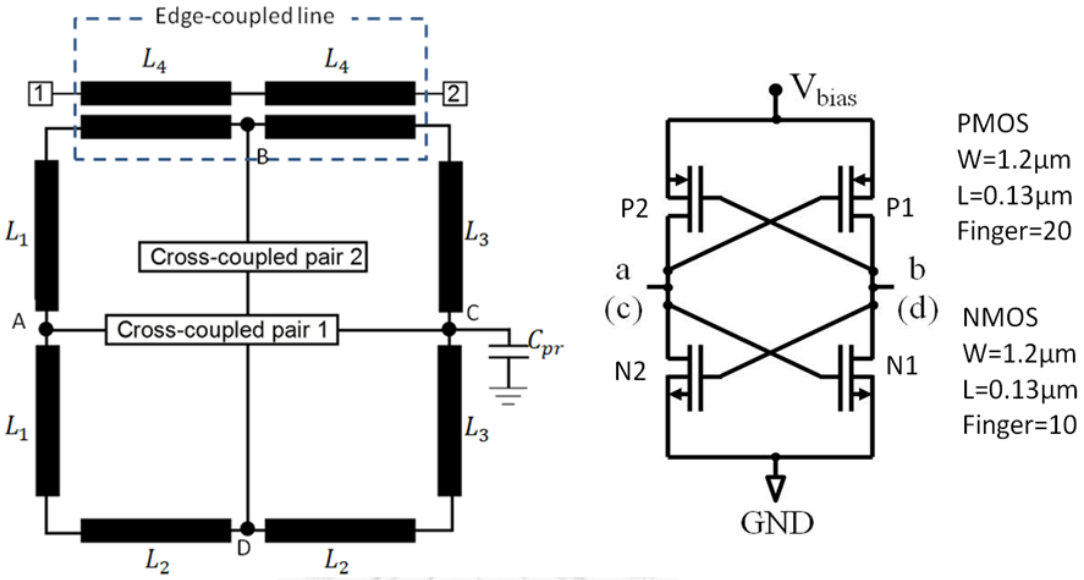

Figure 3.15 (a) The schematic of the bandstop filter. (b) The circuit of the cross-coupled pairs.

Figure 3.16 The equivalent circuit of the dual-mode bandstop filer. L is the group wavelength at the resonance frequency or λ_g.

Figure 3.16 is the total equivalent circuit of the bandstop filter. After the transistor size is chosen, the characteristic of the coupled line should be decided. Figure 3.17 shows the coupled line structure which used in this design. The coupled line is laid on the top metal layer, and two coupled lines are almost symmetric. The even and odd mode characteristic impedance is found by full-EM simulation on Ansys HFSS with Agilent Advanced Design System (ADS). The real part of even mode characteristic impedance is $59.5\ \Omega$. The real part of odd mode characteristic impedance is $14.9\ \Omega$. The characteristic impedance of the coupled line is chosen to eliminate the reflection zeros beside the stop band. If the reflection zeros are too near to the resonance frequency, the bandstop effect will degrade.

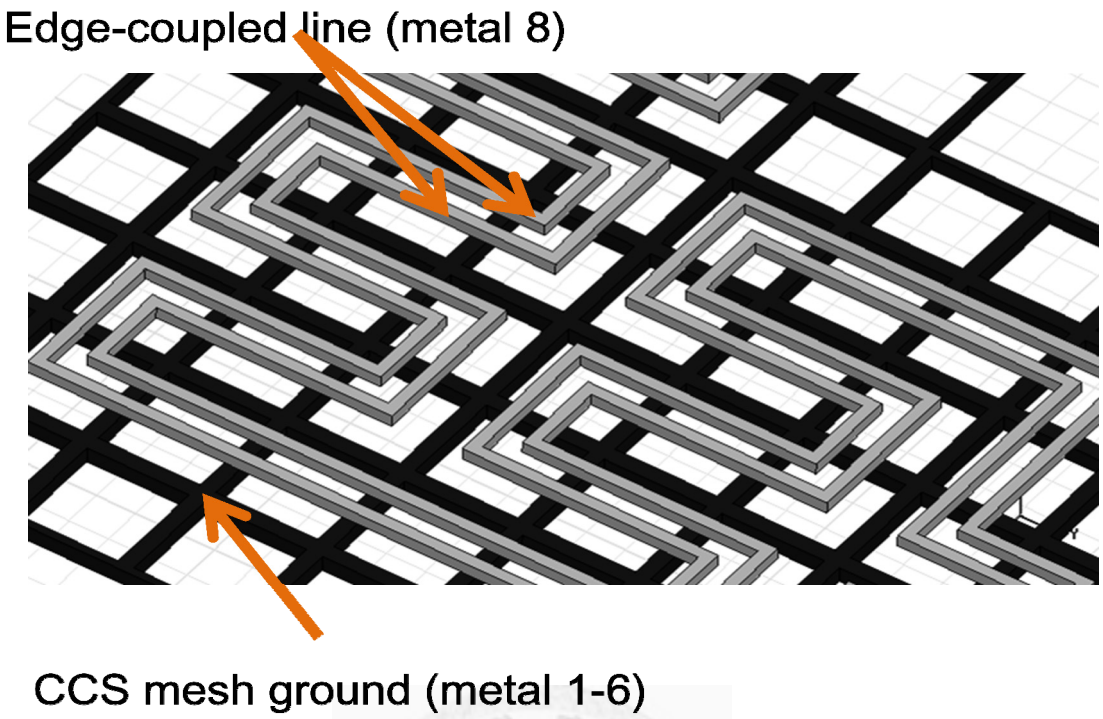

Figure 3.17 The 3D view of the coupled line used in edge-coupled dual-mode bandstop filter.

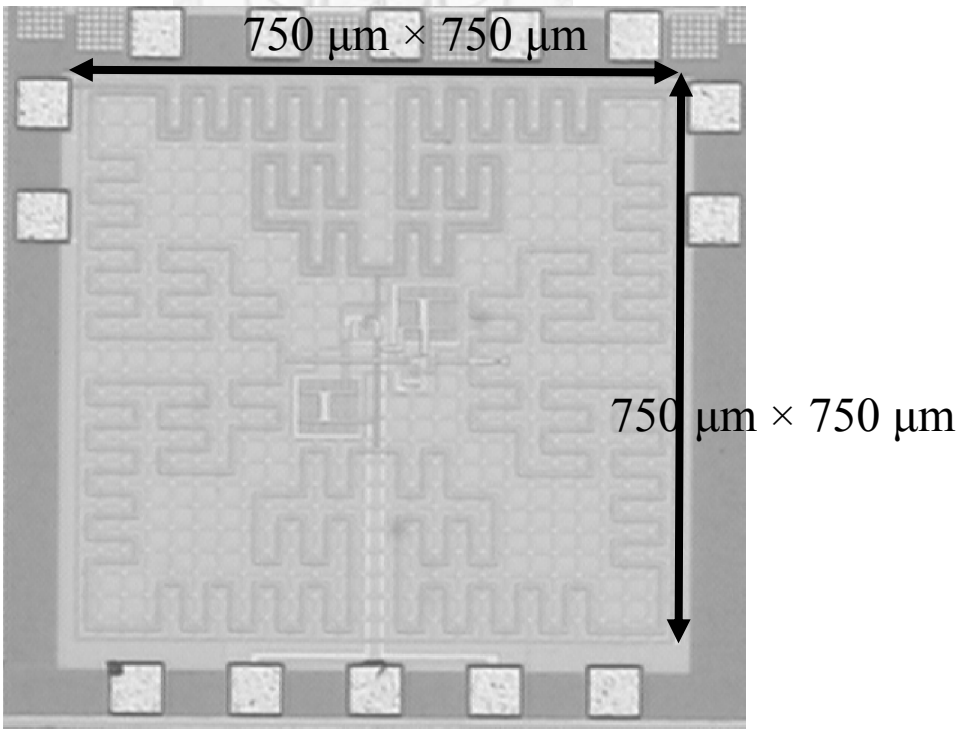

Figure 3.18 The chip photo of the edge-coupled dual-mode bandstop filter.

Figure 3.18 is the chip photo of the bandstop filter. The upper side is the coupled line, the other is transmission lines of the resonator. All the active component is at the middle of the chip.

3.7.2 Measurement Result of Edge-coupled Bandstop Filter

Figure 3.19 shows the $|S_{11}|$and $|S_{21}|$ response from 8GHz to 10GHz. The dotted line is the simulation result from HFSS and ADS. The solid line is the results of on-wafer measurement. The measurement was implemented after on-wafer short-open-load-thru (SOLT) calibration to de-embed the parasitic of the contacting pads. During the measurement, the power level of input signal is set at -25 dB.

The measured central frequency of the dual-mode bandstop filter is 8.60 GHz. The bandwidth is about 0.10 GHz (8.55 GHz to 8.65 GHz) with 10-dB insertion loss. The 10-dB bandwidth is 0.10 GHz (1.16% of fractional bandwidth) and 5-dB bandwidth is 0.16 GHz (1.86% of fractional bandwidth). The deepest rejection in band is -19.7 dB at 8.58 GHz. The in-band return loss is all less than -7.99 dB and has the minimums of 3.09 dB at 8.55 GHz and 3.54 dB at 8.59 GHz.

There are two things that should be discussed for a while. One of them is the reflection zero that occurs beside the stopband in the measurement results but not in the simulation result. The reason for the exist of the zero is the source-load coupled during measurement. This chip is about $720\ \mu m$ wide, which is about 0.26 wavelength in 8.50 GHz. The two probes to touch the pads besides the chip is so closed that small coupling between these two probes occur. Besides, the simulation does not think about the pad effect as well. The zero was initially occur at higher frequency and now be moved adjacent to the stop band. There is an interesting that the two poles of $|S_{11}|$ is not the same frequencies of the zeros of $|S_{21}|$. The poles' position may be affected by

the zero beside the stopband. Since the zero is at the right side of the stop band, the poles of $|S_{11}|$ are slightly move to lower frequency.

The out-band response is shown in Figure 3.20 and Figure 3.21. The out-band insertion loss is 1.31 dB at 6.00 GHz, 1.14 dB at 8.00 GHz, 0.38 dB at 10.00 GHz and 0.25 dB at 12.0 GHz. The 5-dB bandwidth is 0.16 GHz (8.52 GHz to 8.68 GHz). Therefore the skirt factor $SF = 1.6$.

The supplied voltage is 0.937 V and 0.983V for two crossed coupled pair. The currents are both less than $150\mu A$.

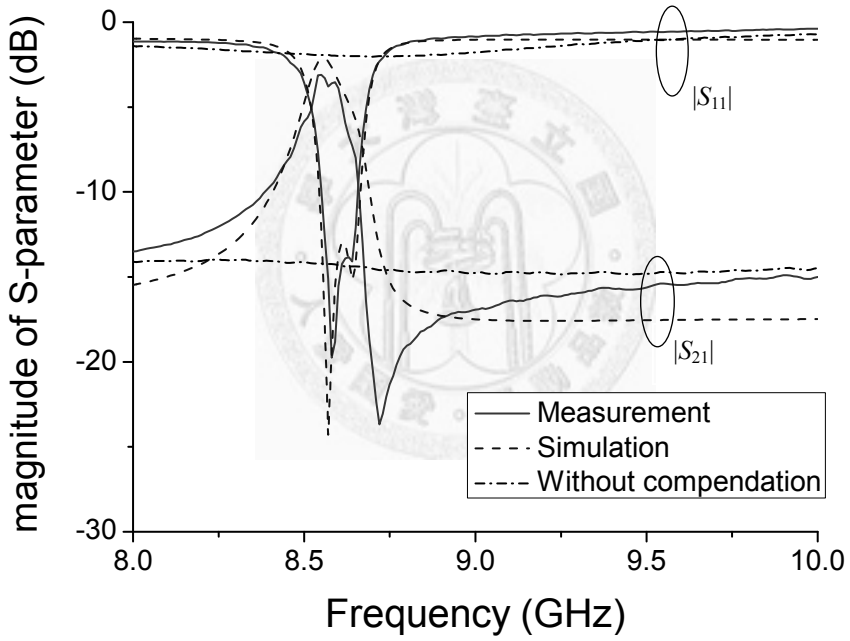

Figure 3.19 $|S_{11}|$ and $|S_{21}|$response of edge-coupled dual-mode bandstop filter.

Figure 3.20 $|S_{11}|$ response from 6 GHz to 12 GHz of edge-coupled dual-mode bandstop filter.

Figure 3.21 $|S_{21}|$ response from 6 GHz to 12 GHz of edge-coupled dual-mode bandstop filter.

3.7.3 Active Dual-mode Bandstop Filter with broadside-coupled line

The bandwidth of the bandstop filter is determined by the coupling strength of the coupled line. The loaded capacitors can only changed the resonant frequency. In the previous design, the bandwidth with 10-dB rejection is 0.89% fractional bandwidth, which is a very narrow bandwidth. However, by the limitation of the fabrication rules, the gap between coupled lines cannot be too small, and the thickness of each layer is unchangeable, which set a limitation for the coupling strength for edge-coupled coupled line. Thus, a dual-mode bandstop filter with broadside coupled is implemented. The two lines of coupled line are laid on metal layer 7 and metal layer 8, respectively. The gap between two lines is now the distance from metal layer 7 to metal layer 8, which is much smaller than the edge-coupled. Besides, by changing the width of the lines, the coupling strength can be adjusted easily. There are also some disadvantages. The coupled line now is a very asymmetric structure, where even mode and odd mode analysis may fail to explain the characteristic of the coupled line. On the other hand, the main signal line is now laid on metal layer 7, which have larger conducting loss and dielectric loss as well. The insertion loss out of the stop band may increase since the cross coupled pair cannot compensate the loss of the signal line. Figure 3.22 is the 3D view of the coupled line. The upper metal layer is laid on metal layer 8, and is used as a part of the ring resonator. The signal line is laid on metal 7. The thickness of metal 7 is much thinner than metal 8, and is more closed to the Silicon substrate as well. Therefore the loss of metal 7 is larger than metal 8. Figure 3.23 is the schematic of this filter, which is almost the same as Figure 3.16. The different parts are the coupled line and the value of the tuning capacitor C_{pr}. Figure Figure 3.24 is the chip photo of the filter.

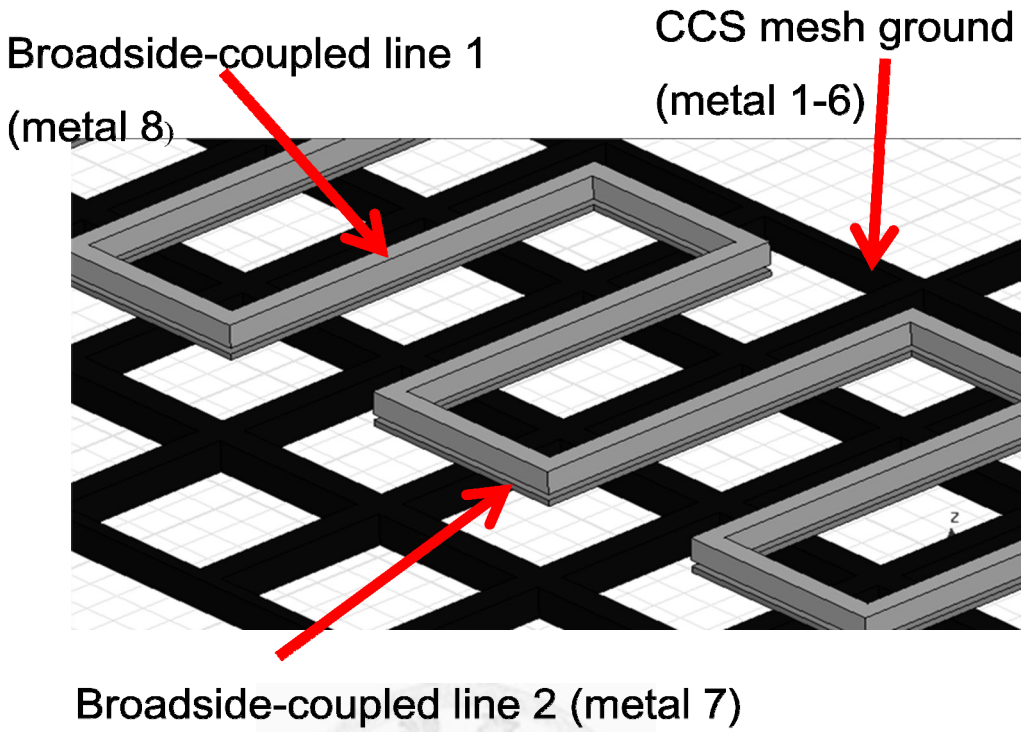

Figure 3.22 The 3D view of the coupled line used in broadside-coupled dual-mode bandstop filter.

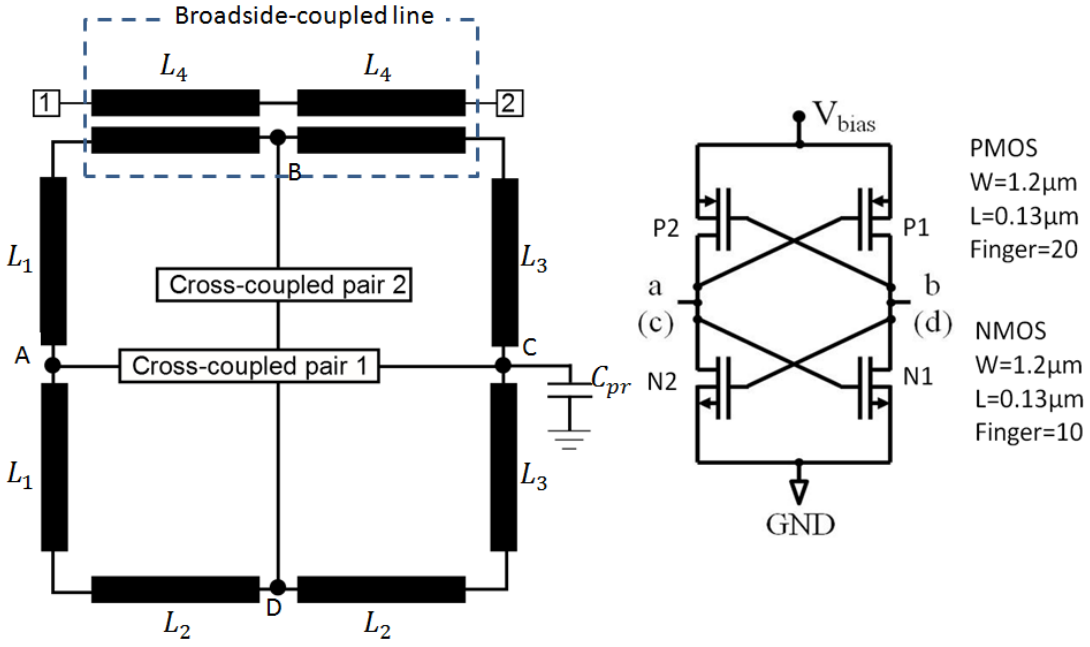

Figure 3.23 Equivalent circuit of the broadside-coupled dual-mode bandstop filter.

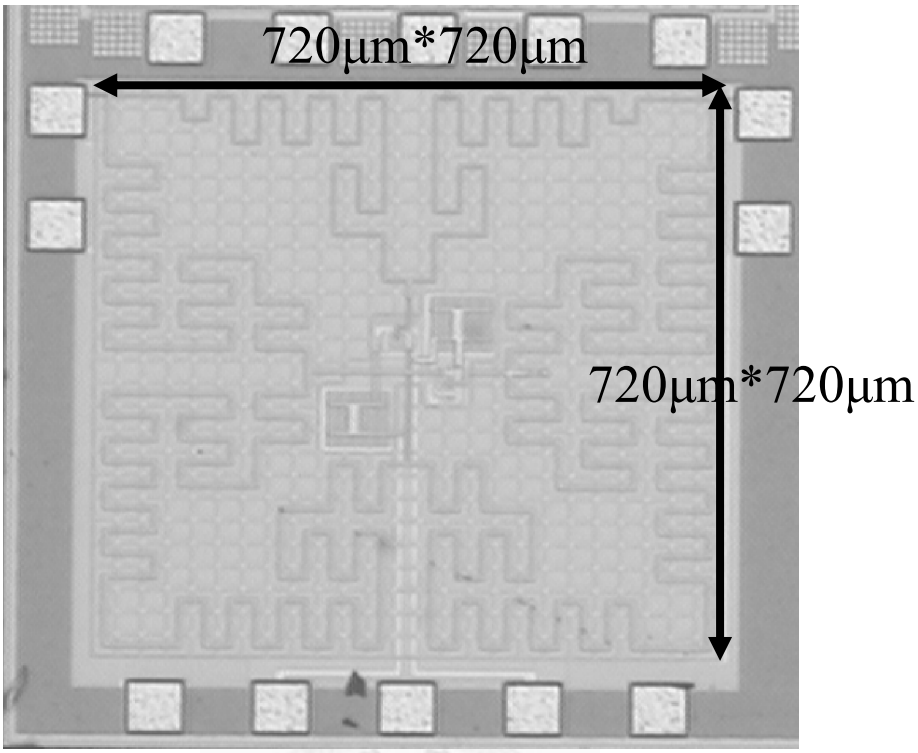

Figure 3.24 The chip photo of the broadside-coupled dual-mode bandstop filter.

3.7.4 Measurement Result of broadside-coupled Bandstop Filter

Figure 3.25 shows $|S_{11}|$ and $|S_{21}|$ response from 8.00 GHz to 10.00 GHz. The dotted line is the simulation result from HFSS and ADS. The solid line is the results of on-wafer measurement. The measured central frequency of the dual-mode bandstop filter is 8.19 GHz. The bandwidth is about 0.49 GHz (7.98 GHz to 8.47 GHz) with 10-dB insertion loss. The 10-dB bandwidth is 0.49 GHz (5.71% for fractional bandwidth). The deepest rejection in band is -23.1 dB at 8.59 GHz. The out-band response is shown in figure 3.21 and figure3.21.

The out-band insertion loss is 5.62 dB at 6.00 GHz, 4.93 dB at 10.00 GHz and 5.2 dB at 12GHz. The 5-dB bandwidth is 0.69 GHz (8.52 GHz to 9.17 GHz). Therefore the skirt factor $SF = 1.41$.

The in-band return loss is less than -7.2 dB for all the bandwidth. The return loss is compensated to 0.00 dB at 7.81 GHz and -2.00 dB at 8.73 GHz.

The supplied voltage is 0.95 V and 0.87 V for two crossed coupled pairs. The currents are both less than 150 μA. There is still something to be discussed. In Figure 3.25, there is a reflection zero at about 6.80 GHz in the measurement result where the zero does not occur in simulation. The reason is the same as the discussion in the section 3.7.2. The reflection zero may occur if there are source-load coupling. In the measurement case, the probes and pads of the chip are very close. The distance between two probes is about 0.75 mm, which is less than a wavelength at this frequency. Besides, there are DC pad laid on the top of the chip, each separated by 0.15 mm. Those are not concerned in the simulation. In fact, each time the probes are put on the pad, the reflection zero position may even change.

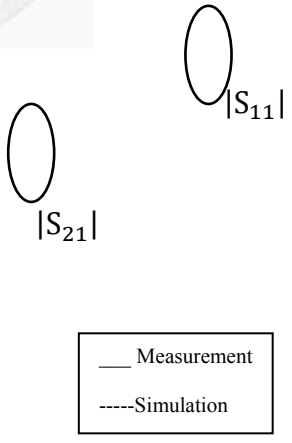

Figure 3.25 $|S_{11}|$ and $|S_{21}|$response of broadside-coupled dual-mode bandstop filter.

Chapter 4 Dual-band Dual-mode Bandstop Filter

In the previous chapter, the background knowledge and method for designing a active dual-mode bandstop resonator on CMOS IC have been introduced. In chapter 2, a dual-band dual-mode bandstop filter has been implemented by C. Karpuz et al. However, the second resonator is put aside from the first one. The area of the filter is actually the sum of two resonators, which is approximately the same as cascading two bandstop filters. However, different from the cascading case, the dual-band dual-mode designs suffer from more complicated issue, like the position of reflection zeros. The study is actually interesting.

The mentioned dual-band dual-mode bandstop filter is implemented on PCB board, which is like the most dual-mode bandstop case. On the other hand, CMOS fabrication offers several metal layers and through vias between each metal layers. The vertical structure is possible if it has been design well. In this chapter, a dual-band dual-mode bandstop filter is implemented on CMOS IC and the area is maintained the same as the single-band dual-mode design in the previous chapter. It actually makes a lot difference to design a circuit on CMOS and on PCB. Moreover, the vertical stacked design introduces even more issues to be studied. In this chapter, the schematic and design flow have been mentioned. All the full-EM simulation is performed by Ansys HFSS with Agilent ADS software to get the simulation result combining passive structure and active circuit. The measurement result is also shown in the last section.

4.1 The Schematic

The schematic of dual-band dual-mode bandstop filter is very similar as Karpuz's. Since the design is implemented on CMOS chip, the active compensating circuit is needed as before. Figure 4.1 is the schematic of the proposed dual-band dual-mode active bandpass filter. Figure 4.1(a) shows two capacitor-perturbed (C_{pr1} and C_{pr2} for each one) and cross-coupled-pair-loaded ring resonators are coupled to a signal to form a bandstop filter. Notice that the two resonators are vertically stacked, and therefore the total area do not increase from the single band case, as shown in Figure 4.1(c). The most of energy passes one of the coupled lines and till some is coupled into these two resonators from the coupled line in the middle. The length of the transmission lines of the lower frequency resonator is $L_1 = 1.98\,\text{mm}$. The coupled line length of two resonators are both $L_2 = L_4 = 0.99\,\text{mm}$.The transmission line length of the higher frequency resonator is $L_3 = 0.54\,\text{mm}$. Since the coupled line length of the two resonator is the same in physical length, the horizontal cross-coupled pair in the high frequency resonator is not loaded at the 90° and 270° of the resonator. Figure 4.1(b) is the cross-coupled pair circuit. P1, P2 are PMOS transistors and N1, N2 are NMOS transistors. The structure is the same as the single mode one. Figure 4.1(c) is the layout of the dual-band dual-mode active bandstop filter. The size of a CCS TL unit cell is $30\mu\text{m} \times 30\mu\text{m}$.

(a) (b)

(c)

Figure 4.1 Schematic of the proposed dual-band dual-mode active bandpass filter. (a) Two capacitor-perturbed (C_{pr1} and C_{pr2} for each one) and cross-coupled-pair-loaded ring resonators are coupled to a signal to form a bandstop filter. The energy passes one of the coupled lines and some is coupled into these two resonators from the coupled line in the middle. $L_1 = 1.98$ mm . $L_2 = L_4 = 0.99$ mm . $L_3 = 0.54$ mm (b) The cross-coupled pair circuit. P1, P2 are PMOS transistors and N1, N2 are NMOS transistors. (c) Layout of the dual-band dual-mode active bandstop filter. The size of a CCS TL unit cell is $30.0\ \mu m \times 30.0\ \mu m$.

4.2 Doubled Layer CCS TL

In section 3.1, the CCS TL used as the transmission line is introduced. The CCS transmission line in the previous design uses metal layer 8 as signal line. The metal layer 1 to metal layer 6 is connected by vias to form a thick metal layer and is used as the ground metal. Since the dielectric loss in CMOS IC is majorly contributed by the loss in the Silicon substrate. A thick ground can enhance the Q factor. Now another resonator is put under the original one. In this design, metal layer 4 and metal layer 5 are connected by vias to be used for the other signal line. To reduce the strong coupling between two signal layers, a mesh ground constructed by combining the metal layer 6 and metal layer 7 are put between two resonators. On the other hand, to reduce the dielectric loss from the Silicon substrate, another mesh ground constructed by metal layer 2 is put under the second signal layer. On every corner of the mesh ground there is a via connecting two ground layer to ensure the integrity of ground. Figure 4.2 is the cross-sectional view of the double layers structure.

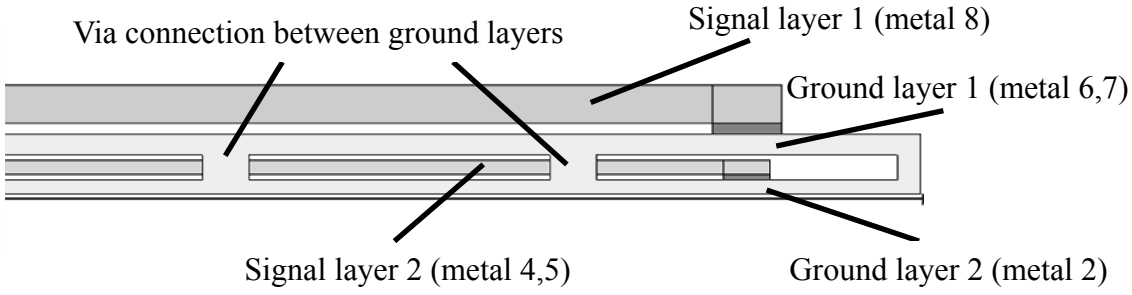

Figure 4.2 The cross-sectional view of the double layers structure.

The CCS TL structure of the signal layer 1 is similar to the microstrip line, while

the in signal layer 2, the structure is more like strip line, with ground are both up and down. On the other hand, to reduce the coupling of two signal layers even more, the transmission lines in signal layer 1 and signal layer 2 layout are designed to be orthogonal in the cross area if possible. Therefore the broadside coupling between signal layer 1 and signal layer 2 is reduced as much as possible. The 3D view of the layout of transmission lines is shown in Figure 4.3.

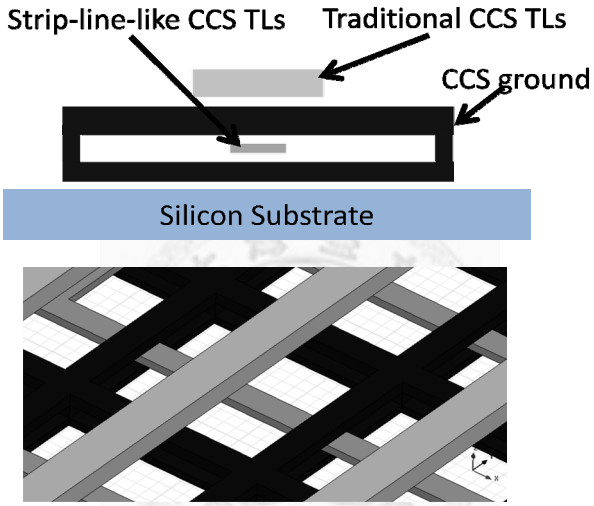

Figure 4.3 The 3D view of the layout of transmission lines.

By the same method mentioned in chapter 3, the parameter of the transmission lines are extracted as fellow:

Signal line 1			Signal line 2		
Z_c	Q	SWF	Z_c	Q	SWF
$40.3 - 1.77j\ \Omega$	6.88	3.07	$42.0 - 3.64j\ \Omega$	3.71	1.74

Table 4.1 The transmission line parameters of two layers

From the table above, the loss of signal line 2 is much bigger than signal one,

since the conduction loss and dielectric loss are both larger than signal line 1 case. The signal line 2 is designed to construct the high frequency resonator because the length of transmission line is shorter.

4.3 Multi-metal Coupled line

Thought the two resonators are stacked vertically, the coupled line is still put on the top metal layer (metal layer 8). The coupled line is designed to be as symmetric as possible. However, it is hard to find out the characteristic impedance of triple coupled line. Figure 4.4 is the 3D-view of the coupled line. The width of each line is 3 μm and the gap between lines is 2 μm, the limitation of fabrication in CMOS 0.13 μm technology.

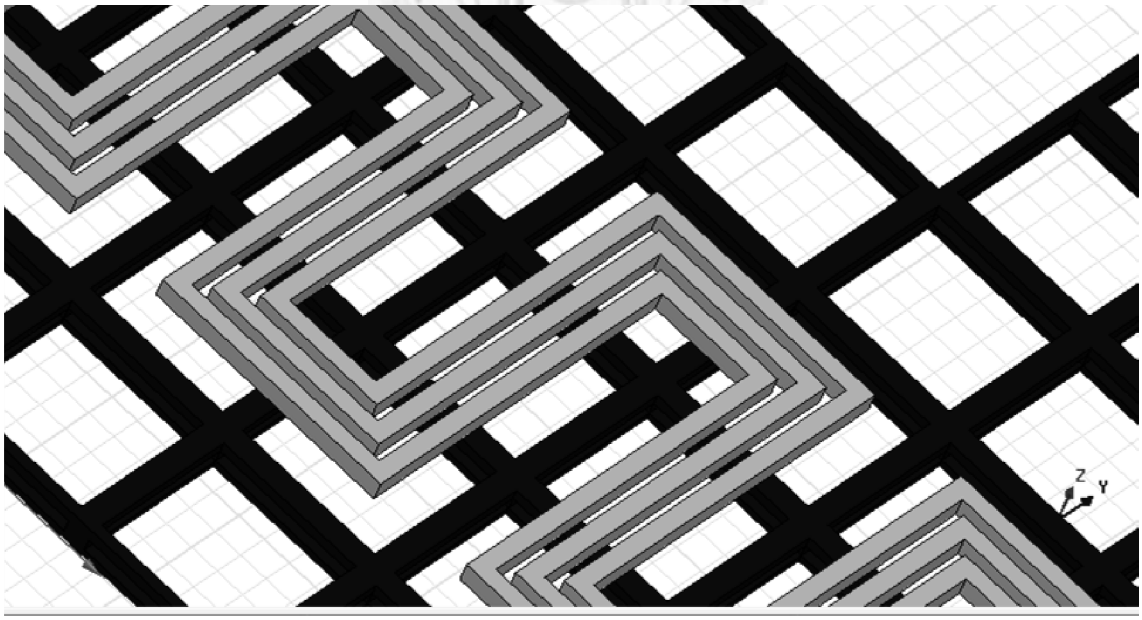

Figure 4.4 The 3D-view of the coupled line.

4.4 Dual-band Dual-mode Bandstop filter Issues

From the discussion in the chapter 2, it can be found that the reflection zeros may be a big trouble if it coincidently lays on the transmission zeros of the other band. The two zeros will be cancelled and we will get a very bad performance. Therefore the parameters of each mode, or each resonator, should be chosen to have no any reflection zero.

In single band case, the cross-coupled pairs are designed to compensate only one mode, respectively. In fact, for any mode, the compensation circuit of the other mode will not work well. Since it is not the resonant frequency of this mode, this mode will not resonate very well, and the two ends of the cross-coupled pair is not purely odd mode. The cross-coupled pair will not work as a good negative resistor. Therefore, the mode with the cross-coupled pair may act as a load at the frequency of the other mode. But in single mode case, this effect is not obviously since the two mode are so adjacent that the cross-coupled pair still work as a negative resistance for both two modes. However, in dual-band case, the resonator with active circuits of the other band acts as a load for this band. This problem shows in the performance of the in-band return loss, as shown in figure 4.6. For a good active bandstop filter, when $|S_{11}|$ is compensated to near 0 dB case, the shape of $|S_{21}|$ will performed a best rejection. If over compensating the resonator, the resonator may act like an oscillator, and $|S_{21}|$ and $|S_{11}|$ will get higher simultaneously, and may larger than 0dB. If there are loads on the signal line, the return loss will not be compensated to zero. If so, the over compensated case is occur, the shape of $|S_{21}|$ will degrade. If the compensation is too large, this structure may oscillate.

Another issue is the insertion loss between two bands. It is shown by simulation that the closer the two band, the higher the insertion between two bands. It is because there are coupling between two resonators. The filter with two bands in fact acts as a high order filter. This effect also shows in figure 4.7 and figure 4.9. Figure 4.5 is the chip photo of the dual-band dual-mode filter. The area of the filter is $910\mu m \times 910\ \mu m$.

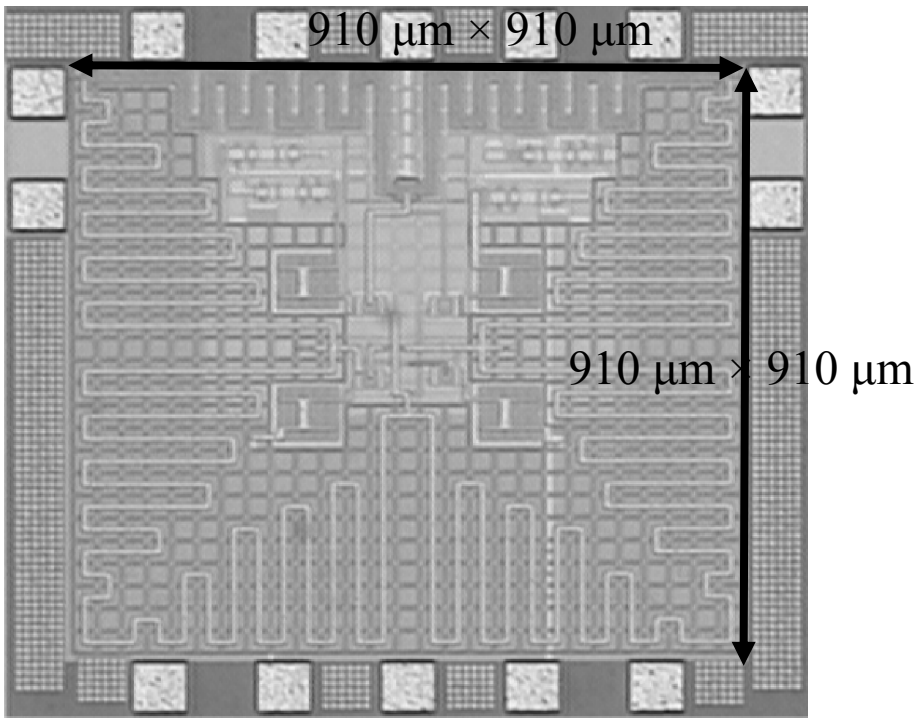

Figure 4.5 The chip photo of the dual-band dual-mode bandstop filter.

4.5 Simulation and Measurement Results

The measurement was implemented after on-wafer short-open-load-thru (SOLT) calibration to de-embed the parasitic of the contacting pads. During the measurement, the power level of input signal is set at -25.0 dB.

There are two designs shown in this thesis. The only difference of this two

designs is the value of the perturbation capacitors. With different perturbation, the mode splitting of each band can be changed.

Figure 4.6 and Figure 4.7 show $|S_{11}|$ and $|S_{21}|$ response from 6.00 GHz to 12.00 GHz of the first design. The dotted line is the simulation result from HFSS and ADS, and the solid line is the measurement result of filter.

For the lower frequency band, the measured central frequency is 7.29 GHz, and the simulated result is 7.42 GHz. The bandwidth is about 0.07 GHz (7.26 GHz to 7.33 GHz) with 10-dB insertion loss. The deepest rejection level is -11.59 dB at 7.29 GHz. Since the $|S_{21}|$ shows no obvious dual mode (no ripple) in this band, the worst case of rejection level is at the side of this band, and is -10dB. The in-band return loss is all less than -7.43 dB and has the minimums of 6.59 dB at 7.23 GHz and 7.41 dB at 7.34 GHz. There is visible ripple in $|S_{11}|$ in this band. The local maximum of return loss in this band is 7.44 dB at 7.31 GHz.

For the higher frequency band, the measured central frequency is 9.64 GHz, and the simulated result is 10.75 GHz. The bandwidth is about 0.51 GHz (9.38 GHz to 9.89 GHz) with 10-dB insertion loss. The deepest rejection level is -25.43 dB at 9.46 GHz and -23.69 dB at 9.85 GHz. There is ripple in this band. The local minimum rejection level is -10.83 dB at 9.68 GHz. The in-band return loss is all less than -10.13 dB. However, since the perturbation capacitor is asymmetric to port 1 and 2, and also the band is affected by the other band, the shapes of $|S_{11}|$ and $|S_{21}|$ are not matched in both two bands. To define the bandwidth from $|S_{11}|$ and $|S_{21}|$ may get different ranges. The minimum return loss is -2.60 dB at 9.42 GHz.

The out-band insertion loss is -4.66 dB at 6GHz, -4.88 dB at 8GHz, -3.39 dB at 12GHz.

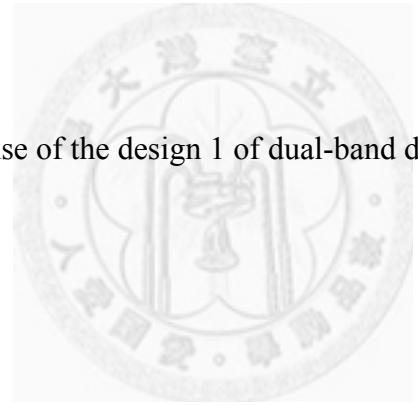

Figure 4.6 $|S_{11}|$ response of the design 1 of dual-band dual-mode bandstop filters.

Figure 4.7 $|S_{21}|$ response of the design 1 of dual-band dual-mode bandstop filters.

Figure 4.8 and Figure 4.9 show the $|S_{11}|$and $|S_{21}|$ response from 6GHz to 12GHz of the second design. The dotted line is the simulation result from HFSS and ADS, and the solid line is the measurement result of filter.

This filter is designed to show obvious dual-mode characteristic for both bands. Since the bandwidth of each mode is very narrow, for any band the rejection level in the middle is very bad(less than -10dB). This filter can be viewed as a forth band bandstop filter implemented by two dual mode resonator.

For the lower frequency band, the measured central frequency is 7.17 GHz, and the simulated result is 7.32 GHz. The deepest rejection level is -29.63 dB at 7.01 GHz and -21.66 dB at 7.32 GHz. In the rejection band, the worst rejection level is -3.42 dB at 7.15 GHz. The in-band return loss has the minimums of 1.61 dB at 7.01 GHz and 0.95 dB at 7.27 GHz. There is visible ripple in $|S_{11}|$ in this band. The local maximum of return loss in this band is 3.46 dB at 7.13 GHz.

For the higher frequency band, the measured central frequency is 9.74 GHz, and the simulated result is 10.69 GHz. The deepest rejection level is -27.64 dB at 9.49 GHz and -28.66 dB at 10.03 GHz. There is ripple in this band. The local minimum rejection level is -7.76 dB at 9.8 GHz. The minimum return loss is -2.81 dB at 9.49 GHz and -2.67 dB at 10.07 GHz. The out-band insertion loss is -2.42 dB at 6.00 GHz, -3.23 dB at 8.00 GHz, -2.86 dB at 12.00 GHz.

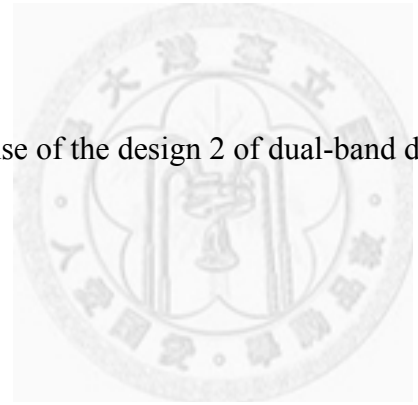

Figure 4.8 $|S_{11}|$ response of the design 2 of dual-band dual-mode bandstop filters.

Figure 4.9 $|S_{21}|$ response of the design 2 of dual-band dual-mode bandstop filters.

Chapter 5 Conclusion

5.1 Discussion and Summary of the Designs

In this thesis, some designs of active dual-mode bandstop filter are proposed. The first design is the edge-coupled dual-mode bandstop filter. The second design is the broadside-coupled dual-mode bandstop filter. The third is the vertical stacked dual-band dual-mode filter. All of these filters share the same schematic, with some difference in coupling strength, perturbation value and transmission lines. Table 5.1 shows the three type dual-mode filters and their S-parameter responses implemented in this paper. The chip area is $750\,\mu m \times 750\,\mu m$ without pads for single band case and $910\,\mu m \times 910\,\mu m$ dual-band.

Type	Edge-coupled dual-mode filter	Broadside-coupled dual-mode filter	Dual-mode dual-band fitler
	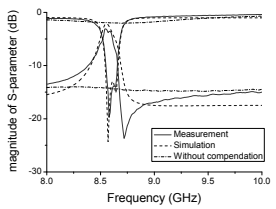		

Table 5.1 The three type dual-mode filters and their S-parameter responses.

5.2 Future Work

In this thesis, a very narrow bandwidth active dual-mode bandstop filter is proposed. However, the rejection level is still not exiting. The design of multi-order filters with multiple resonators coupled to one another may be a good idea to achieve this goal. On the other hand, there are still some spaces to be improved in dual-band dual-mode bandstop filters. One of which is the insertion loss in the stop band. As discussed in chapter 4, the other resonator is a load in the stop band. Also, the compensation techniques can only compensate the resonators in the resonating case. The signal line suffers from the same problem of poor Q factor, which is not compensated by active circuit either. The insertion loss out of the stop band is not so good compared to PCB case. This increases the noise figure in the whole system. Therefore, the compensation of the signal line is a subject to be studied in the future too. Third, the linearity issue of these designs is a problem and a more stably controlled cross-coupled pair, maybe with a feedback circuit to improve the linearity is another great issue.

Reference

[1] I. Wolff, "Microstrip bandpass filter using degenerate modes of a microstrip ring resonator," *ELectron. Lett.,* vol. 8, pp. 302-303, 1972.

[2] M. Guglielmi and G. Gatti, "Experimental Investigation of Dual-Mode Microstrip Ring Resonators," in *Europe. Microw. Conf.*, 1990, pp. 901-906.

[3] H. Chien-Hsun, F. Lu, and C. Kai, "Slotline annular ring elements and their applications to resonator, filter and coupler design," *IEEE Trans. Microw. Theory Tech.,* vol. 41, pp. 1648-1650, 1993.

[4] H. Jian-Sheng, H. Shaman, and C. Young-Hoon, "Dual-Mode Microstrip Open-Loop Resonators and Filters," *IEEE Trans. Microw. Theory Tech.,* vol. 55, pp. 1764-1770, 2007.

[5] L. Zhu, P. M. Wecowski, and K. Wu, "New planar dual-mode filter using cross-slotted patch resonator for simultaneous size and loss reduction," *IEEE Trans. Microw. Theory Tech. on,* vol. 47, pp. 650-654, 1999.

[6] J. A. Curtis and S. J. Fiedziuszko, "Miniature dual mode microstrip filters," in *IEEE MTT-S Int. Microw. Symp. Dig.*, 1991, pp. 443-446 vol.2.

[7] S. Saxena, S. Porwal, K. Soni, P. Chhawchharia, and S. K. Koul, "Novel tunable bandstop filter using E-shaped dual mode resonator," in *Microwaves, Communications, Antennas and Electro. Systems, COMCAS. IEEE Int. Conf. on*, 2009, pp. 1-5.

[8] S. Saxena, S. Porwal, K. Soni, P. Chhawchharia, and S. K. Koul, "Analysis and design of bandstop filter using E-shaped dual mode resonator," in *Microwaves, Communications, Antennas and Electro. Systems, COMCAS. IEEE Int. Conf. on*, 2009, pp. 1-6.

[9] J. Wang, L. Ge, K. Wang, and W. Wu, "Compact microstrip dual-mode dual-band bandpass filter with wide stopband," *ELectron. Lett.,* vol. 47, pp. 263-265, 2011.

[10] C. Xin-Kai, X. Jun, and Z. Min, "Miniature dual-mode bandpass filters using hexagonal open-loop resonators with E-shaped stubs loading," in *Signals Systems and Electron. Int. Symp. on*, 2010, pp. 1-3.

[11] K. Yi-Ting and C. Chi-Yang, "Analytical Design of Two-Mode Dual-Band Filters Using E-Shaped Resonators," *IEEE Trans. Microw. Theory Tech.,* vol. 60, pp. 250-260, 2012.

[12] B. Wise, "Active bandpass and bandstop filters using identical networks," *ELectron. Lett.,* vol. 5, pp. 366-367, 1969.

[13] U. Karacaoglu, I. D. Robertson, and M. Guglielmi, "A dual-mode microstrip ring resonator filter with active devices for loss compensation," in *IEEE MTT-S Int. Microw. Symp. Dig.*, 1993, pp. 189-192 vol.1.

[14] L. Su and C. K. C. Tzuang, "A Narrowband CMOS Ring Resonator Dual-Mode Active Bandpass Filter With Edge Periphery of 2% Free-Space Wavelength," *IEEE Trans. Microw. Theory Tech. ,* vol. 60, pp. 1605-1616, 2012.

[15] H. Jia-Sheng and L. Shuzhou, "Dual-mode microstrip triangular patch resonators and filters," in *IEEE MTT-S Int. Microw. Symp. Dig.*, 2003, pp. 1901-1904 vol.3.

[16] H. Jia-Sheng and L. Shuzhou, "Theory and experiment of dual-mode microstrip triangular patch resonators and filters," *IEEE Trans. Microw. Theory Tech.,* vol. 52, pp. 1237-1243, 2004.

[17] H. Jia-Sheng, "Microstrip dual-mode band reject filter," in *IEEE MTT-S Int. Microw. Symp. Dig.*, 2005, p. 4 pp.
[18] X. Jian-Kang and H. Hui-Fen, "New microstrip filter using single right-angled triangular patch resonator," in *Microw., Antenna, Propagation and EMC Technologies for Wireless Communications, 2009 3rd IEEE Int. Symp. on*, 2009, pp. 1167-1170.
[19] H. K. Chiou and C. F. Tai, "Dual-band microstrip bandstop filter using dual-mode loop resonator," *ELectron. Lett.,* vol. 45, pp. 507-509, 2009.
[20] J. S. Hong and M. J. Lancaster, "Bandpass characteristics of new dual-mode microstrip square loop resonators," *ELectron. Lett.,* vol. 31, pp. 891-892, 1995.
[21] C. Karpuz, A. Gorur, E. Gunturkun, and A. K. Gorur, "Asymmetric response dual-mode dual-band bandstop filters having simple and understandable topology," in *Proc. Asia-Pacific Microwave Conf.*, 2009, pp. 925-928.
[22] C. Chih-Chiang and C. K. C. Tzuang, "Synthetic quasi-TEM meandered transmission lines for compacted microwave integrated circuits," *IEEE Trans. Microw. Theory Tech.,* vol. 52, pp. 1637-1647, 2004.
[23] W. Sen, T. Kun-Hung, C. Meng-Ju, W. Hsien-Shun, and C. K. C. Tzuang, "Super Compact Miniaturization of CMOS RFICs Using Synthetic Quasi-TEM Transmission Lines," in *Art of Miniaturizing RF and Microwave Passive Components, 2008. IMWS 2008.* , 2008, pp. 94-97.
[24] C. K. C. Tzuang, W. Hsien-Hung, W. Hsien-Shun, and J. Chen, "CMOS Active Bandpass Filter Using Compacted Synthetic Quasi-TEM Lines at Band," *IEEE Trans. Microw. Theory Tech.,* vol. 54, pp. 4548-4555, 2006.
[25] H. Kuo-Ken, C. Meng-Ju, and C. K. C. Tzuang, "A 3.3 mW K-Band 0.18-um 1P6M CMOS Active Bandpass Filter Using Complementary Current-Reuse Pair," *IEEE Microw. Wireless Compon. Lett.,* vol. 18, pp. 94-96, 2008.
[26] L. Meng-Lin, W. Hsien-Shun, and C. K. C. Tzuang, "1.58-GHz Third-Order CMOS Active Bandpass Filter With Improved Passband Flatness," *IEEE Trans. Microw. Theory Tech.,* vol. 59, pp. 2275-2284, 2011.
[27] A. Gorur, "Description of coupling between degenerate modes of a dual-mode microstrip loop resonator using a novel perturbation arrangement and its dual-mode bandpass filter applications," *IEEE Trans. Microw. Theory Tech.,* vol. 52, pp. 671-677, 2004.
[28] S. Amari, "Comments on "Description of coupling between degenerate modes of a dual-mode microstrip loop resonator using a novel perturbation arrangement and its dual-mode bandpass filter applications"," *IEEE Trans. Microw. Theory Tech.,* vol. 52, pp. 2190-2192, 2004.
[29] G. M. A. Eryilmaz, G. B. Elif, G. C. Adnan, and K. D. Ceyhun, "Dual-mode microstrip bandstop filters," in *Proc. Asia-Pacific Microwave Conf.*, 2008, pp. 1-4.